Published online 22 May 2021

Nucleic Acids Research, 2021, Vol. 49, No. 10 ***5967–5984***
https://doi.org/10.1093/nar/gkab387

The DNA binding domain of the *Vibrio vulnificus* SmcR transcription factor is flexible and binds diverse DNA sequences

Jane D. Newman[1,2], Meghan M. Russell[1], Lixin Fan[3], Yun-Xing Wang[3], Giovanni Gonzalez-Gutierrez[2] and Julia C. van Kessel[1,*]

[1]Department of Biology, Indiana University, 1001 E 3rd St, Bloomington, IN 47405, USA, [2]Department of Molecular and Cellular Biochemistry, Indiana University, 212 S Hawthorne Dr, Bloomington, IN 47405, USA and [3]Small Angle X-ray Scattering Facility, Center for Structural Biology, National Cancer Institute, National Institutes of Health, Frederick, MD 21702, USA

Received February 22, 2021; Revised April 23, 2021; Editorial Decision April 27, 2021; Accepted April 28, 2021

ABSTRACT

Quorum sensing gene expression in vibrios is regulated by the LuxR/HapR family of transcriptional factors, which includes *Vibrio vulnificus* SmcR. The consensus binding site of *Vibrio* LuxR/HapR/SmcR proteins is palindromic but highly degenerate with sequence variations at each promoter. To examine the mechanism by which SmcR recognizes diverse DNA sites, we generated SmcR separation-of-function mutants that either repress or activate transcription but not both. SmcR N55I is restricted in recognition of single base-pair variations in DNA binding site sequences and thus is defective at transcription activation but retains interaction with RNA polymerase (RNAP) alpha. SmcR S76A, L139R and N142D substitutions disrupt the interaction with RNAP alpha but retain functional DNA binding activity. X-ray crystallography and small angle X-ray scattering data show that the SmcR DNA binding domain exists in two conformations (wide and narrow), and the protein complex forms a mixture of dimers and tetramers in solution. The three RNAP interaction-deficient variants also have two DNA binding domain conformations, whereas SmcR N55I exhibits only the wide conformation. These data support a model in which two mechanisms drive SmcR transcriptional activation: interaction with RNAP and a multi-conformational DNA binding domain that permits recognition of variable DNA sites.

INTRODUCTION

Bacterial pathogens oscillate between vastly different environments outside and within their host organism. Cells must tune gene expression to respond to changes such as nutrient acquisition, temperature, pH, salt and the presence of other microorganisms. Upon entering a host, bacteria need to upregulate genes required for colonization and establishing an infection, including cell surface appendages for attachment to surfaces, secretion systems for delivery of toxins, and enzymes for digestion of macromolecules for nutrient acquisition (1–5). Vibrios are Gram-negative bacteria that are found in the marine environment, and many of these bacteria are also pathogens of a variety of fish and shellfish (6–10). Notably, some vibrios are potent human pathogens such as *Vibrio cholerae*, *Vibrio parahaemolyticus* and *Vibrio vulnificus*. In vibrios, one major regulatory system that controls expression of virulence genes is quorum sensing.

Quorum sensing is a process of cell–cell signaling that allows bacteria to control group behaviors in response to an increase in population density (11–13). Quorum-sensing transcription factors are responsible for regulating hundreds of genes. In *Vibrio* species, the master quorum-sensing transcriptional regulators are the LuxR/HapR/SmcR-type proteins that are produced at high cell density (14,15). In vibrios, these proteins are the central regulators of virulence gene expression, including LuxR in *Vibrio harveyi* and *Vibrio alginolyticus*, HapR in *V. cholerae*, OpaR in *V. parahaemolyticus*, and SmcR in *V. vulnificus*. Indeed, deletion or inhibition of *smcR* in *V. vulnificus* decreases pathogenesis in both mouse and shrimp models (16,17). Thus, these core regulatory proteins are central to our understanding of the influence of quorum sensing on virulence. We note that *V. harveyi* BB120 has been reclassified as *Vibrio campbellii* BB120 (a.k.a. ATCC BAA-1116) (18), but we refer to this organism in this manuscript as *V. harveyi* for consistency with the literature (19–21).

Among vibrios, *V. vulnificus* is considered a potent human pathogen due to a mortality rate of greater than 50%

*To whom correspondence should be addressed. Tel: +1 812 856 2235; Email: jcvk@indiana.edu

in primary septicemia infection cases (22). In *V. vulnificus*, the master quorum-sensing transcription factor SmcR is responsible for activating virulence genes via many factors, one of which is by increasing the expression of an elastase gene *vvpE* by directly binding to the promoter (23). It is hypothesized that this activation mechanism functions via SmcR interaction with RNA polymerase (RNAP). A direct interaction between LuxR and RNAP alpha in *Vibrio harveyi* has been shown *in vitro* and *in vivo* (24), and this interaction with RNAP also exists with SmcR (25).

Transcriptional activation in bacteria canonically occurs via interactions with RNAP via recruitment or stabilization of RNAP interactions with DNA (26,27). Conversely, repression generally occurs through blocking key promoter elements or binding of required activator proteins (28,29). The complexity of these processes in bacteria has recently become more fully appreciated with the advent of deep-sequencing technologies and the ability to connect transcriptomics to nucleoprotein complexes at promoters (30,31). Such experiments have revealed numerous important aspects of the mechanism of regulation by the LuxR/HapR/SmcR family of transcription factors. These proteins are completely different from the LuxI/LuxR quorum-sensing systems that synthesize and directly bind autoinducers, respectively, to enable DNA binding and regulation. Rather, LuxR/HapR/SmcR are sub-members of the broader TetR family of transcription factors. Previous work has shown that these quorum-sensing regulators are distinct from most TetR proteins because they have no known ligand and they are able to activate and repress transcription of many genes, while most TetR proteins only repress 1–2 genes with a few exceptions (32,33). Similar to most TetR proteins, the binding consensus sequences for LuxR/HapR/SmcR proteins tends to be between 20 and 22 bp long (34–36). In contrast to typical TetR proteins, the site for LuxR/HapR/SmcR is quite degenerate (34,36–38). The diverse binding sites of the LuxR/HapR/SmcR group also have a wide array of binding affinities, with dissociation constants ranging from ∼0.5–100 nM (37). Though a significant portion of biochemistry has been performed with the founding member of this family, *V. harveyi* LuxR, the *V. vulnificus* SmcR protein is highly amenable to structural studies by X-ray crystallography (39). The *V. cholerae* HapR protein has also been amenable to crystallography (40), but the DNA-binding domain of LuxR and SmcR are 100% identical whereas there are some differences in HapR (Supplementary Figure S1A), making the study of SmcR more appealing for studying DNA-binding mechanisms. Thus, we focus on the mechanisms of transcriptional activation by the *V. vulnificus* TetR-type protein SmcR.

TetR proteins exist in different conformational states: apo, ligand-bound or DNA-bound (41). Generally, ligand binding increases the separation of the DNA binding domains compared to the DNA-bound form of the protein. For example, superimposition of the apo, ligand-bound and DNA-bound crystal structures of TetR shows that the DNA binding domain has a pendulum-like shift of 2.7–7.5 Å (41). While there is substantial crystallography evidence supporting this pendulum-like shift in several TetR protein family members, the field would benefit from further investigation of this shift using biophysical assays of proteins in solution. The general 'Ω'-shaped quaternary structure of TetR proteins is highly conserved, even though primary amino acid sequences can be divergent (41,42). Specifically, the sequence identity in the ligand binding domain region is highly variable, thus allowing for the recognition of diverse molecules in different TetR proteins. Although a native ligand has not been identified for LuxR/HapR/SmcR proteins, there is a hypothetical ligand binding domain in the C-terminus that has been shown to interact with chemical inhibitors (17,39). There are also multiple examples of TetR proteins that bind DNA as dimers-of-dimers in which the two dimers do not interact but bind the major grooves on opposite sides of the DNA helix (43–46). Further, one TetR-type protein, EthR from *Mycobacterium tuberculosis*, has been shown to bind DNA with one, two or three dimers per DNA substrate (47). The observation of higher-order structures in some TetR-type proteins introduces the question of whether the *Vibrio* TetR proteins also form higher-order structures.

The transcription field has historically used mutational analysis to separate the functions of DNA binding and protein-protein interactions involved in transcription initiation (48–50). Indeed, positive control mutants that disrupt protein-protein interactions but retain DNA binding activity provide important insights into the functional mechanisms employed by transcription factors. Here, we examine separation-of-function mutants to investigate SmcR-DNA and SmcR-protein interactions and the impact of these functions on activation of quorum-sensing genes. Our data show that a specific amino acid substitution in the DNA binding domain of SmcR renders the protein incapable of binding DNA at most binding sites. Conversely, positive control amino acid substitutions in the RNAP interaction domain of SmcR do not alter the conformations of the DNA binding domains. Our results support a model that multiple conformations of SmcR allow recognition of diverse DNA binding sequences in activated quorum-sensing promoters.

MATERIALS AND METHODS

Bacterial strains and media

Escherichia coli strains DH10B and S17-1λpir were used for cloning, and BL21(DE3) was used for overexpression of proteins (Supplementary Table S1). All *E. coli* strains and derivatives were grown in Lysogeny Broth (LB) at 30°C shaking at 275 RPM in LB media with the corresponding antibiotic. *V. vulnificus* ATCC 27562 and derivatives were grown shaking at 275 RPM at 30°C in Luria Marine (LM) medium (LB with 2% NaCl) with appropriate antibiotics (Supplementary Table S1). Antibiotics were used at the following concentrations: kanamycin 50 μg/ml or 250 μg/ml (*E. coli* or *V. vulnificus*, respectively), chloramphenicol 10 μg/ml, ampicillin 100 μg/ml and tetracycline 10 μg/ml. The dual promoter fluorescence reporter assays were performed using plasmid pJV064 containing the P_{luxC} fused to GFP and P_{05222} fused to mCherry to assess LuxR transcriptional regulation. Overnight *E. coli* cultures containing *luxR* and the dual fluorescence reporter were diluted 1:1000, induced with 15.6 μM IPTG, and grown for 16 h at 30°C.

The OD_{600} and fluorescence (both GFP and mCherry) was measured on a BioTek plate reader.

Molecular methods

PCR was performed using Phusion HF polymerase purchased from New England Biolabs (NEB). T4 polynucleotide kinase (T4 PNK) used in EMSAs and all other enzymes mentioned were purchased from NEB and used according to manufacturer's instructions. Site-directed mutagenesis for overexpression of mutant proteins was carried out using the Agilent QuikChange II XL Site-Directed Mutagenesis Kit. The mutations were confirmed by DNA sequencing (Eurofins). All oligonucleotides were purchased from Integrated DNA Technologies (IDT), and those used in this study are listed (Supplementary Table S3). Cloning details for plasmids listed in Supplementary Table S2 are available upon request.

RNA analysis by qRT-PCR

To collect RNA samples, cells were grown at 30°C shaking at 275 RPM to an OD_{600} of approximately 0.2. Then cells were induced with 50 μM IPTG and grown under the same conditions until cells reached an OD_{600} of ∼1, at which 5 ml of cells were collected by centrifugation and frozen in liquid N_2. RNA was extracted using a Trizol/chloroform extraction protocol previously described (51) and cleaned up using an RNeasy Mini Kit (Qiagen). Quantitative real-time PCR (qRT-PCR) was performed as previously described (52). Samples were normalized to the internal standard *recA* gene. The $\Delta\Delta C_T$ values were used to analyze data from three independent biological replicates. Symbols on graphs represent the mean values and error bars represent the standard deviations. All statistical analysis was performed with functions from GraphPad Prism version 8. Further details are available in the figure legends.

Protein purification

SmcR and RNAP alpha proteins were purified similarly to previous publications with minor adjustments (24,37,53). *Escherichia coli* BL21(DE3) strains containing plasmids expressing hexahistidine-tagged *smcR* wild-type and mutant alleles were grown overnight in LB medium with kanamycin, back-diluted 1:100 into 1 l of LB medium with kanamycin, and grown to an OD_{600} of 0.4–0.6 at 30°C. Expression of SmcR was induced by IPTG to a final concentration of 1 mM and cultures grown for 4 h shaking at 30°C. The cells were pelleted and frozen at –80°C. The pellet was resuspended in 25 ml buffer A (25 mM Tris pH 8, 500 mM NaCl), and an Avestin EmulfiFlex-C3 emulsifier was used to lyse cells. The soluble lysate was applied to a HisTrap HP Ni-NTA column using an Äkta Pure FPLC in buffer A and eluted from the column with a gradient of buffer B (25 mM Tris pH 8, 500 mM NaCl, 1 M imidazole). The purified protein was concentrated to ∼5 ml using Sartorius Vivaspin Turbo 10 000 MWCO centrifugal concentrators. The sample was manually injected into the Äkta Pure and separated via size exclusion chromatography on a HiLoad™ 16/600 Superdex™ 75 pg column equilibrated with gel filtration buffer (25 mM Tris pH 7.5, 200 mM NaCl). Eluted fractions were analyzed by SDS-PAGE, pooled, and concentrated using the same centrifugal concentrators previously mentioned. The samples were then immediately used in crystal trays or frozen in liquid nitrogen with a final concentration of 10% glycerol and stored at –80°C. All SmcR proteins used in Bio-layer Interferometry (BLI) experiments and SmcR N55I for crystallography was overexpressed in *E. coli* BL21(DE3) using the Intein Mediated Purification with an Affinity Chitin-binding Tag (IMPACT) system utilizing the pTXB1 vector for a C-terminal tag. Cells were grown and induced the same as previously stated, pelleted, and resuspended in buffer 1 (25 mM Tris pH 8, 500 mM NaCl, 1 mM EDTA) prior to lysis by an Avestin EmulfiFlex-C3 emulsifier. The soluble lysate was applied to NEB chitin resin in buffer 1. The resin was washed with 10 CV buffer 1 and 10 CV buffer 2 (25 mM Tris pH 8, 1 M NaCl, 1 mM EDTA) then incubated with 30 ml buffer 1 and 231 mg dithiothreitol (DTT) for 4 h to promote self-cleavage of the intein tag from the SmcR proteins. The protein cleaved from the intein-tag was eluted with buffer 1 and dialyzed for 2 h in gel filtration buffer. The dialyzed fractions were then concentrated to ∼3 ml and manually injected into the Äkta Pure and separated via size exclusion chromatography on a HiLoad™ 16/600 Superdex™ 75 pg column equilibrated with gel filtration buffer. The purification of his-tagged *V. harveyi* RNAP alpha was previously described (24).

Crystallization and structure determination of SmcR variants

SmcR wild-type and variants were crystallized in conditions similar to those previously described (39) with slight variations. SmcR WT and variants (∼4 mg/ml) crystals grew at 20°C using the hanging-drop vapor-diffusion method. Crystals formed under the condition of 0.2 M of lithium sulfate, 0.1 M imidazole buffer pH 7.6–8, and 6–10% PEG3350. Then, crystals were harvested, cryo-protected in reservoir solution supplemented with 20% ethylene glycol or a mix of 10% glycerol and 10% ethylene glycol and flash-frozen in liquid nitrogen. Diffraction data were collected at 100 K at the Beamline station 4.2.2 at the Advanced Light Source (Berkeley National Laboratory, CA, USA) and were indexed, integrated, and scaled using XDS (54). The structures were solved by molecular replacement using PHASER and the PDB code 3KZ9 (only one chain) as a search model. The Autobuild function was used to generate a first model that was improved by iterative cycles of manual building in Coot (55) and refinement using PHENIX (56). MolProbity software (56) was used to assess the geometric quality of the models and Chimera (57) or Pymol (58) to generate molecular images. Data collection and refinement statistics are indicated in Supplementary Table S4. All data sets but variant N55I (space group C2) were initially processed in space group $P2_12_12_1$. Data presented translational pseudo-symmetry (as defined by Xtriage in Phenix), patterson peaks with length larger than 15 Å and pseudo-translation vector (0.234, 0.5, 0.0). As a result, multiple molecular replacement solutions with high TFZ and LLG were obtained, most of them with *R*-free values over 0.34 after refinement. Then, data sets were reprocessed in lower symmetry space groups. All solutions

from molecular replacement, in every possible space group, were built and refined using Maximum Likelihood (ML) and Least Squares (LS) as target functions. Those with the best R factors were achieved in space group $P2_12_12_1$ and using ML method (Supplementary Table S4). Translational non-crystallography correction was not used during refinement, since it had marginal effect, if any, on *R* values. UCSF Chimera software was utilized to superimpose structures using the matchmaker function and then distances between alpha carbons were calculated. These were calculated using the following command: distance #1.1 :5.a@CA #2.1 :5.a@CA. This comparison was done for each residue present in the solved structures. Chimera was also used to display crystal contacts shown in figures, as well as measure the distances of these putative contacts. This was done using the Tools: Higher-Order Structure function and selecting Multiscale Models. Then with loaded atoms and contact distance near a set range of 5 Å, select the Multimer 3 × 3 × 3 crystal unit cells and make models. Then clashes/contacts can be utilized from the structural analysis function in tools. The parameters used for contacts was the default criteria: VDW overlap = –0.4 Å and subtract 0 from overlap for potentially hydrogen-bonding pairs. All protein structures in figures were produced using Chimera software.

Radiolabeling DNA probes and electrophoretic mobility shift assays (EMSAs)

The EMSAs were conducted in a similar fashion to previous publications (24,52). The oligonucleotides used as substrates were annealed in 1× annealing buffer (50 mM Tris–HCl pH 7.5, 100 mM NaCl) at 95°C for 1 min then cooled from 95 to 10°C at 1°C/min to generate dsDNA substrates. The 500 nM annealed DNA substrates were then radiolabeled in PNK buffer with PNK enzyme and radioactive ATP [γ^{32}P] from Perkin Elmer at 37°C for 1 h then diluted in TE buffer (10 mM Tris, 1mM EDTA pH 8). The excess ATP [γ^{32}P] was removed using GE Healthcare G-25 columns. The final dsDNA concentration of the probes was 5 nM. EMSAs were carried out as previously described (52) with a dilution series of protein (specified in figure legends), 10 ng/μl poly(dI:dC), 100 μg/ml bovine serum albumin (BSA), 1× binding buffer (10 mM HEPES pH 7.5, 100 mM KCl, 2 mM DTT, 2 mM EDTA) for 30 min at 30°C. Protein–DNA complexes were visualized on TGE (25 mM Tris, 250 mM glycine, 1 mM EDTA) polyacrylamide gels in TGE buffer. Gels were dried for 1 h at 80°C then exposed to a phosphor screen and analyzed on a Typhoon 9210 (Amersham Biosciences).

Bio-layer interferometry

Bio-layer interferometry (BLI) was performed according to protocols previously established (24). BLI was performed on an Octet® K2 System using Dip and Read™ Ni-NTA (NTA) Biosensors (FortéBio®). In a 96-well plate, the interaction of untagged SmcR proteins (WT or N55I) were assayed with 200 nM his-tagged *V. harveyi* RNAP alpha subunit. His-tagged Tobacco etch virus (TEV) protease was used as a control for non-specific interactions (24). The reactions were carried out in SmcR gel filtration buffer (25 mM Tris pH 7.5, 200 mM NaCl) with various concentrations (1000, 850, 700, 550, 400, 250 and 0 nM) of the SmcR protein (*i.e.,* the analyte). The method on the Octet® K2 System Data Acquisition 9.0 software was set up to perform 30 s sensor equilibration in the reference well, 300 s ligand-loading step in the ligand-loading well, 60 s baseline step in the reference well, 700 s association step in the association well, and 700 s dissociation step in the reference well. All steps were performed shaking at 30°C for each concentration of analyte. The data were analyzed using Octet® K2 System Data Analysis 9.0 software.

Small angle X-ray scattering (SAXS)

SAXS measurements were carried out at the 12ID-B beamline of the Advanced Photon Source (APS), Argonne National Laboratory. Photon energy was 13.3-keV and sample-to-detector distance was 1.9 m to achieve a useable q range of $0.005 < q < 0.88$ Å^{-1}, where $q = (4\pi/\lambda)\sin\theta$, and 2θ is the scattering angle. Concentration series measurements for wild-type SmcR and SmcR N551 solutions were carried out. The concentrations were 1, 2 and 4 mg/ml for SmcR and SmcR N551 in buffers consisting of 200 mM NaCl and 25 mM Tris pH 7.5 (SmcR) or 200 mM NaCl, 25 mM Tris pH 7.5, 1 mM DTT, 0.5 mM EDTA (SmcR N55I). Forty-five 2D images were recorded with a Pilatus 2 M pixel detector for each matching buffer and sample solution using a flow cell, with the exposure time of 0.5–1 seconds to minimize radiation damage and get good signal-to-noise ratio. The 2D images were corrected and reduced to 1D scattering profiles using the Matlab scripts at the beamlines. The 1D SAXS profiles were grouped by sample and averaged, followed by buffer background subtraction.

The radius of gyration (R_g) and intensity at zero angle $I(0)$ were generated from Guinier plots in the range of $qR_g < 1.3$. For comparison, R_g and $I(0)$ were also calculated in real and reciprocal spaces using program GNOM in q range up to 0.30 Å^{-1} (59). The pair—distance distribution function $P(r)$ and maximum dimension (D_{max}) were also calculated using GNOM. The molecular weights were estimated based on the method of correlation volume, V_c (60), and the Bayesian statistics method (61). The obtained structural parameters and molecular weights are shown in Supplementary Table S5. It was found that the oligomerization status depends on the concentration. Wild-type SmcR at a concentration of 4 mg/ml and SmcR N551 at 1 mg/ml are dominated by dimers. Therefore, these data were selected for fitting to crystal structures. The fitting of an experimental scattering curve from a multiple conformation (oligomer) mixture and determination of volume fractions of each conformation in the mixture were done using OLIGOMER (62).

RESULTS

The N55I substitution in SmcR separates activation and repression phenotypes

The LuxR/HapR/SmcR proteins are of interest because they both activate and repress transcription, which is rare among the TetR family of transcription factors. Previously,

genetic screens have been performed to find separation-of-function mutants of LuxR in order to study the mechanisms of activation or repression individually (37). Substitutions of specific amino acids in the DNA binding domain of LuxR in *V. harveyi* (e.g. N55I; Figure 1A) render the protein unable to bind to specific DNA binding sites, thus resulting in lack of either activation or repression of *V. harveyi* promoters (37). In addition, substitutions in alpha helices 4 and 7 of LuxR (S76A, N142D, L139R) result in decreased or eliminated activation activity due to loss of interaction(s) with RNAP (Figure 1A), and as such are called positive control mutations (24). Because SmcR shares 100% amino acid identity with LuxR in the DNA binding domain, shares 92% identity overall, and contains the same critical residues in the RNAP interaction domain (Supplementary Figure S1A), we hypothesized that substitutions in the same positions in SmcR would yield similar activation- and repression-specific phenotypes. We specifically focused on SmcR N55I for several reasons: (i) the S76A, N142D and L139R substitutions were shown to have the same *in vivo* phenotypes in both LuxR (*V. harveyi*) and HapR (*V. cholerae*), indicating that the interaction with RNAP alpha is conserved across vibrios (24), (ii) the LuxR N55I protein is defective at DNA binding activity at specific sequences but not all known binding sites (37), (iii) the LuxR N55I substitution had the largest decrease in activation activity while retaining wild-type repression activity (37), (iv) the asparagine is in a region of the DNA binding domain that is completely conserved in all LuxR/HapR-type proteins but not *E. coli* TetR and (v) substitution of N55 with four other amino acids (Y, K, S, A) all resulted in loss of activation (32,37). We assayed function of SmcR N55I using a previously published dual-promoter reporter plasmid containing the activated promoter P_{luxC} driving expression of *gfp* and the repressed promoter P_{05222} driving expression of *mCherry* (37). As we predicted, the N55I substitution in SmcR resulted in complete loss of activation of the *luxC* promoter, whereas repression was maintained and even increased compared to wild-type SmcR (Figure 1B).

Our previous work with LuxR/HapR had revealed the RNAP interaction domain on LuxR and established that LuxR interacts with RNAP alpha (24). We used biolayer interferometry (BLI) to show that SmcR also interacts with *Vibrio* RNAP alpha ($K_D = 142 \pm 6$ nM, Figure 1C) with a similar affinity to LuxR ($K_D = 139 \pm 19$ nM). This is the first definitive *in vitro* experiment showing that SmcR and RNAP directly interact. We also observed that SmcR N55I interacts with RNAP alpha ($K_D = 160 \pm 3$ nM) with an affinity similar to wild-type SmcR (Figure 1D). From these data, we conclude that the N55I substitution in the DNA binding domain of SmcR results in a loss of transcription activation that is not caused by a disruption in the RNAP alpha-interaction domain on SmcR.

SmcR N55I has limited DNA binding site recognition

To examine the diversity of sequences bound by SmcR N55I, we assayed DNA binding activity at the eight binding sites A-H in the *luxC* promoter from *V. harveyi* using electrophoretic mobility shift assays (EMSAs). This promoter is ideal for this experiment because the LuxR binding sequence of each of these sites has been determined, and SmcR binds to each of these sites with similar affinity to LuxR (Figure 2A, B, Supplementary Figure S2A) (52). SmcR N55I only binds well to sites B and H, at which it retains near wild-type levels of DNA binding (Figure 2B, Supplementary Figure S2A, S2B, Table 1). The deficient binding of SmcR N55I to six out of eight P_{luxC} binding sites correlates to the lack of SmcR N55I activation activity at the *luxC* promoter *in vivo* (Figure 1B). We note that some EMSA DNA substrates (e.g. sites D and E) migrate differently at high concentrations of SmcR protein that produce quantifiable DNA shifts (Supplementary Figure S2A). These high-migrating substrates do not match the migration pattern of single-dimer shifted bands (e.g. sites A, B, C, F, G, H; Supplementary Figure S2A), and these substrate-specific shifted bands are also observed with LuxR (52). Sites D and E overlap by six basepairs (Supplementary Figure S1B) (52). For each site, we used substrates that contained mutations in the other binding site that we have shown eliminate or greatly decrease binding of LuxR (Supplementary Figure S1B). However, we suspect that these high-migrating bands comprise the binding of a second SmcR dimer to the mutual half-site that is still intact, which is why they are only observed for sites D and E and only at high concentrations that we previously did not test. Another hypothesis is that upon substrate binding SmcR may alter the DNA conformation in a way that changes the migration pattern (e.g. DNA bending) or that a larger protein complex comprised of SmcR tetramers may be forming on the DNA.

To examine differences between the sites, we focused on sites B and H because we observed that the SmcR N55I mutant has similar binding activity to wild-type at these sites (Figure 2B, Table 1). Using the LuxR DNA binding site consensus (previously generated via MEME analysis of ChIP-seq data (37)) as a guide, we aligned the sequences of LuxR binding sites in the *luxC* promoter to identify any sequence patterns that might contribute to binding differences between B and H and the other sites (Figure 2C). We noted that several sites contained substitutions at highly conserved positions in the consensus, such as the T4 and A17 sites. To test the importance of these nucleotides, we introduced substitutions in the sequence of site E (A17→T or T4→A, or both) so that it more closely resembles site B and the consensus (Figure 2C, E). The single nucleotide substitutions each increase wild-type SmcR binding to the substrates compared to wild-type site E but have little to no effect on SmcR N55I binding (Figure 2E). Rather, both substitutions are required to restore SmcR N55I binding to wild-type levels at site E (Figure 2E, Table 1). The single- and double-substitution substrates also substantially increase wild-type SmcR binding affinity for site E (Figure 2B, E, and Table 1). In addition, although this has not yet been formally tested, we note that at position 11, the three sites with the worst binding affinities have a G, whereas the other 5 have an A at that position. Collectively, these data suggest that positions T4 and A17 (and possibly T/A11) are important for stringent SmcR DNA binding.

An interesting characteristic of the LuxR-family degenerate consensus sequence is that it is comprised of a combination of activated and repressed sites (37). It has been previously published that analysis of binding sites in pro-

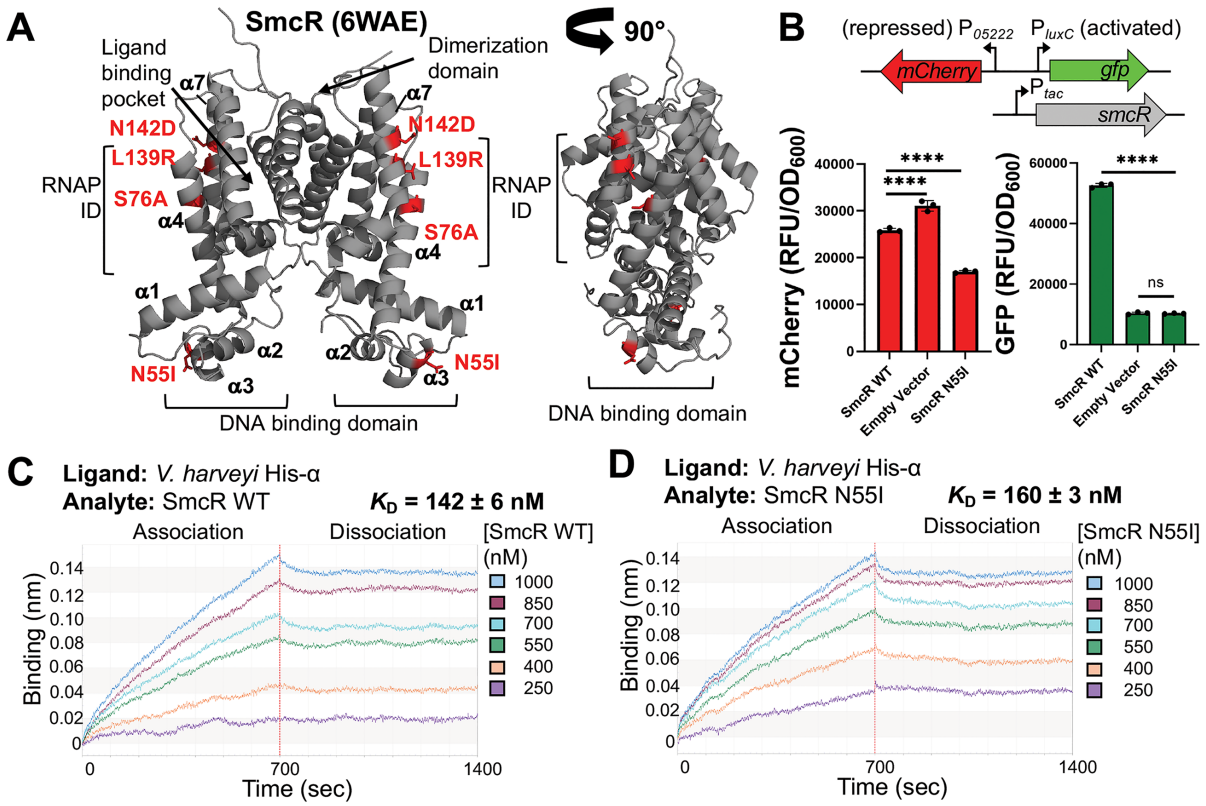

Figure 1. The SmcR N55I substitution mutant is deficient in transcriptional activation but not RNAP interaction. (**A**) X-ray structure of SmcR (PDB: 6WAE) in gray, with relevant substitution mutant residues (N55I, S76A, L139R, N142D) highlighted in red sticks. RNAP ID, RNA polymerase interaction domain. Alpha helices are indicated with numbers. **(B)** Fluorescence (GFP/OD_{600} or $mCherry/OD_{600}$) was measured from biological triplicates of *E. coli* strains containing two plasmids: (i) a dual reporter plasmid pJV064 containing P_{05222}-mCherry (repressed promoter) and P_{luxC}-GFP (activated promoter) and (ii) a plasmid expressing IPTG-inducible copies of either *smcR* (pJN22), the substitution mutant *smcR N55I* (pJN27), or an empty vector control (pMMB67EH-kanR). Asterisks (****) indicate that the fluorescence values are significantly different than the wild-type counterpart ($P < 0.0001$; two-way analysis of variance (ANOVA), followed by Tukey's multiple-comparison test; $n = 3$). (**C**, **D**) BLI analysis of binding reactions containing 200 nM *V. harveyi* His-RNAP alpha (ligand) and the indicated concentrations of analyte wild-type SmcR (C) or SmcR N55I (D). The average calculated binding affinities with standard deviations (K_D; $n = 3$) are listed.

moters repressed by LuxR generates a consensus binding site with dyad symmetry with inverted repeats (Figure 2A) (37). Conversely, sites associated with activated genes generates a consensus site with asymmetry; only one side of the palindrome is conserved (Figure 2D). Thus, the combination of activated and repressed sites is what produces an asymmetric palindrome motif (Figure 2B). However, the critical nucleotides in the consensus site have not been tested in a thorough manner, and thus, our data contribute to our knowledge of this sequence. We note that the sequences recognized by SmcR N55I, including the P_{05222} site and the modified P_{luxC} site E, closely resemble the consensus for repressed binding sites (Figure 2C). Conversely, SmcR N55I does not bind to sites that deviate from the repressed site consensus, such as most other sites in the *luxC* promoter (Supplementary Figure S2B). These results are consistent with new findings of recently solved crystal structures of *V. alginolyticus* LuxR bound to repressed and activated DNA sites; N55 residues from both monomers of the dimer interact with bases in the repressed site (31). However, at an activated DNA site, the N55 residue on one monomer interacts with the DNA, whereas the N55 residue on the other monomer does not (31). From these data, we conclude that SmcR N55I binds to a limited and specific subset of DNA sequences.

SmcR N55I has reduced DNA binding and transcription activation at the vvpE promoter in *V. vulnificus*

We next wanted to study the relevance of the SmcR N55I substitution within the context of *V. vulnificus.* To examine the effects of the N55I substitution on SmcR transcriptional regulation *in vitro* and *in vivo* in *V. vulnificus*, we first used EMSAs to examine DNA binding at promoters in the SmcR quorum-sensing regulon. Two well-studied promoters from *V. vulnificus* were selected: P_{vvpE}, which drives expression of elastase and is activated by SmcR, and P_{vvpM}, which drives expression of a metalloprotease and is repressed by SmcR (63,64). Purified SmcR N55I binds to the *vvpM* promoter with a similar affinity compared to wild-type SmcR, whereas SmcR N55I shows substantially decreased binding to the *vvpE* promoter compared to wild-type (Figure 3A). Alignment of the *vvpE* and *vvpM* binding sites to the consensus sequences shows that they most closely resemble the activated and repressed consensuses, respectively (Figure 2C, D). These results support our conclu-

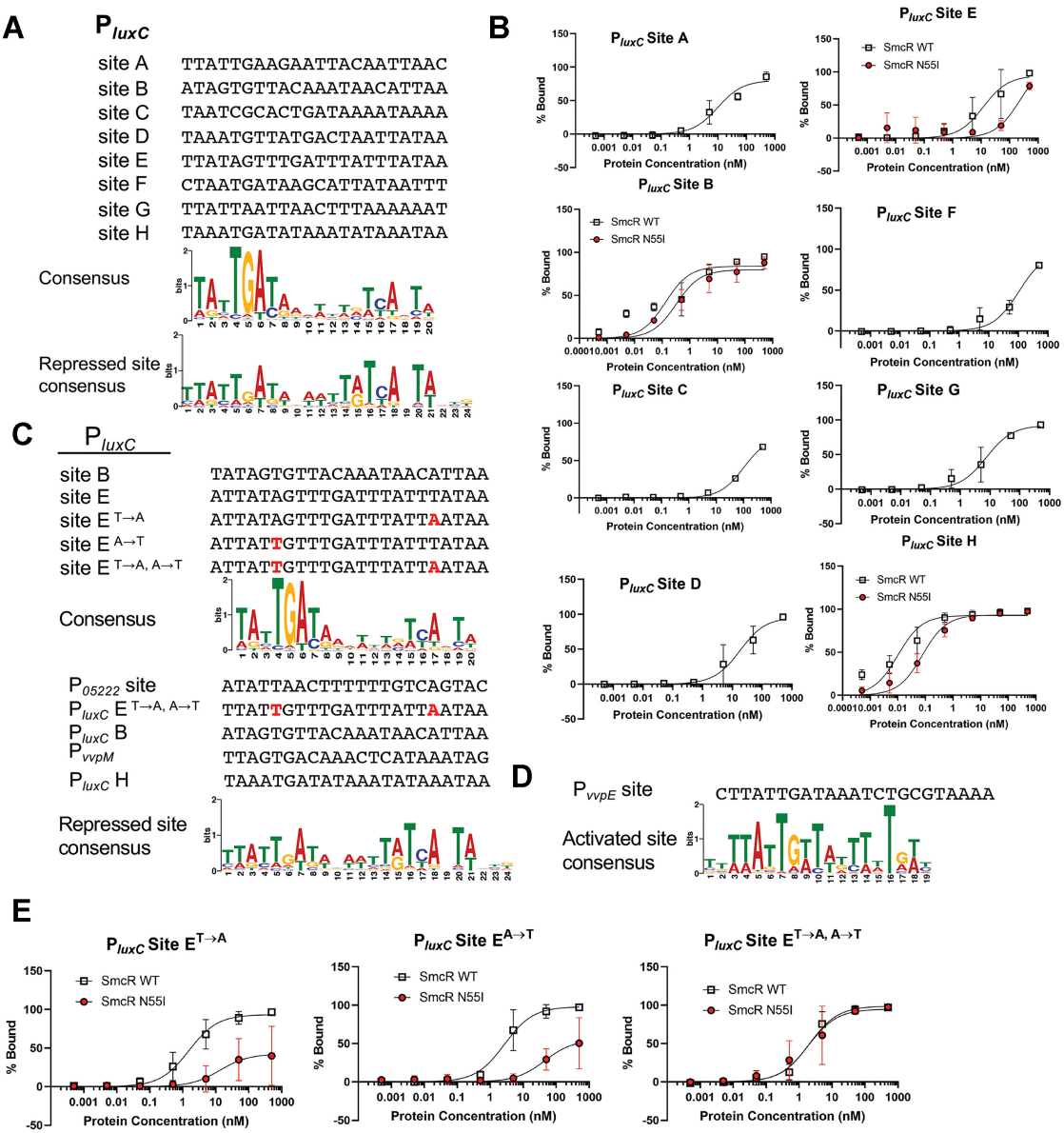

Figure 2. SmcR mutant N55I has limited DNA binding activity. (**A**) Alignment of P_{luxC} binding sites compared to the LuxR consensus binding sequence and the LuxR repressed binding site sequence, which was generated from the subset of LuxR repressed binding sites (37). (**B**) EMSA reactions consisting of 0.5 nM radiolabeled DNA substrates (P_{luxC} binding sites A through H, oligonucleotides listed in Table 1) and purified SmcR wild-type (white squares) or SmcR N55I protein (red circles) with increasing concentrations (0.0005, 0.005, 0.05, 0.5, 5, 50, 500 nM protein). Note that substrates for which no quantifiable shifts were observed for SmcR N55I do not have data points on graphs (Supplementary Figure S2A). Data points show the average of three independent experiments, and error bars indicate the standard deviation. (**C**) (top) Alignment of P_{luxC} binding sites B, E and substitutions made in site E compared to LuxR consensus motif and (bottom) alignment of P_{luxC} binding sites B, $E^{T\rightarrow A,\ A\rightarrow T}$, H, P_{05222} and P_{vvpM} compared to the LuxR repressed consensus motif (37). Mutations in sites are indicated in red text. (**D**) P_{vvpE} binding sites aligned with the LuxR consensus motif for activated sites (37). (**E**) EMSAs comparing SmcR WT and SmcR N55I binding at P_{luxC} binding sites $E^{T\rightarrow A}$, $E^{A\rightarrow T}$ and $E^{T\rightarrow A,\ A\rightarrow T}$ (oligonucleotides listed in Table 1 with increasing protein concentrations (0.0005, 0.005, 0.05, 0.5, 5, 50, 500 nM protein concentrations)).

sion that SmcR N55I functions at repressed promoter sites but has limited or non-functional binding at some activated promoter sites.

We next assayed for transcription activation and repression activity at these promoters *in vivo* using qRT-PCR. The *smcR* or *smcR* N55I genes were expressed in a Δ*smcR* strain on an exogenous plasmid under control of a P_{tac} promoter, thus expression is induced by IPTG. Upon addition of 50 μM IPTG, expression of SmcR or SmcR N55I completely represses *vvpM* (Figure 3B). However, while wild-type SmcR activates *vvpE* compared to the empty vector control strain, SmcR N55I does not increase *vvpE* expression, suggesting that it is not capable of activating the *vvpE* promoter (Figure 3C).These data further support our conclusion that SmcR N55I is defective at binding specific DNA binding sites.

Table 1. EMSA analyses of SmcR protein–DNA interactions

DNA substrate	Oligos	SmcR protein	K_D (nM)
P_{vvpE}	AB324/AB325	WT	2.180
P_{vvpE}	AB324/AB325	N55I	141.5
P_{vvpE}	AB324/AB325	S76A	0.3629
P_{vvpE}	AB324/AB325	L139R	3.529
P_{vvpE}	AB324/AB325	N142D	6.676
P_{vvpM}	AB316/AB317	WT	0.1435
P_{vvpM}	AB316/AB317	N55I	0.2659
P_{vvpM}	AB316/AB317	S76A	0.1666
P_{vvpM}	AB316/AB317	L139R	0.3221
P_{vvpM}	AB316/AB317	N142D	0.5676
P_{luxC} Site B	JDN54/JDN55	WT	0.1311
P_{luxC} Site B	JDN54/JDN55	N55I	0.3222
P_{luxC} Site H	JCV369/JCV620*	WT	0.009997
P_{luxC} Site H	JCV369/JCV620*	N55I	0.07784
P_{luxC} Site E (abolish D binding)	RC212/RC213*	WT	11.98
P_{luxC} Site E (abolish D binding)	RC212/RC213*	N55I	240.6
P_{luxC} Site $E^{T\rightarrow A}$	JDN44/JDN45	WT	1.534
P_{luxC} Site $E^{T\rightarrow A}$	JDN44/JDN45	N55I	13.41
P_{luxC} Site $E^{A\rightarrow T}$	JDN46/JDN47	WT	2.714
P_{luxC} Site $E^{A\rightarrow T}$	JDN46/JDN47	N55I	44.61
P_{luxC} Site $E^{T\rightarrow A,\ A\rightarrow T}$	JCV1107/JCV1108	WT	2.045
P_{luxC} Site $E^{T\rightarrow A,\ A\rightarrow T}$	JCV1107/JCV1108	N55I	1.909
P_{luxC} Site A	JCV1075/JCV1076*	WT	9.944
P_{luxC} Site C	JCV1079/JCV1080*	WT	103.2
P_{luxC} Site D (abolish E binding)	RC224/RC225*	WT	17.96
P_{luxC} Site F	JCV1087/JCV1088*	WT	104.8
P_{luxC} Site G	JCV367/JCV619*	WT	7.558

*Indicates this oligonucleotide pair was published in a previous study (52).

The DNA-binding domain of wild-type SmcR exists in at least two conformations

We hypothesized that differences in the phenotypes observed between wild-type SmcR and the SmcR N55I proteins are due to structural differences in the DNA binding domains. We also predicted that any conformational changes would be subtle because the N55I mutant retains the ability to bind to a small subset of SmcR binding sites (Figure 2A, Supplementary Figure S2A). In order to examine any differences between the structures, we first used X-ray crystallography to examine the structure of wild-type 6Xhis-tagged SmcR. The wild-type SmcR structure that we generated (6WAE; resolution 2.1 Å), as well as the published SmcR structure (3KZ9; resolution 2.1 Å) both have two dimers in the asymmetric unit (space group $P2_12_12_1$; Figure 4A) (39). Although our SmcR 6WAE structure contains a 19-residue N-terminal His-tag (for which no density is observed in the structure), it can be superimposed with the untagged SmcR structure with an average distance between alpha carbons (Cα) of 0.2 Å (Supplementary Figure S3). Throughout this manuscript, we refer to our His-tagged protein simply as SmcR and the previously solved untagged structure as SmcR 3KZ9. To quantify any differences between the two SmcR structures, we plotted the distances between alpha carbons of the four monomers for each of the two structures: SmcR A to SmcR 3KZ9 A, SmcR B to SmcR 3KZ9 B, SmcR C to SmcR 3KZ9 C, and SmcR D to SmcR 3KZ9 D (Supplementary Figure S3B, C). No major variations are observed in any of the four monomers alignments, with the exception of unstructured regions (e.g. the N- and C-termini, Supplementary Figure S3C). We conclude from these data that the presence of the His-tag in the wild-type SmcR structure that we generated does not significantly affect the secondary structure.

We next aligned the two SmcR dimers from the same asymmetric subunit by aligning the AB dimer to the CD dimer. The two dimers are remarkably similar except for two alpha helices and a loop in the DNA binding domain of one monomer that have a distinct shift (Figure 4C). This shift exists in both wild-type SmcR structures: the His-tagged structure 6WAE and the previously solved SmcR 3KZ9 (Supplementary Figure S4A, B). We observe that the distances between DNA binding domain residues in the different dimers vary. For example, the distance between residue 55 in chain A and residue 55 in chain B of the AB dimer is 44.015 Å; whereas the distance between the same residues in the CD dimer is 46.578 Å (Figure 4B). While this 2.6 Å change is not the largest observed (Figure 4C), it is representative of the changes seen along the alpha helices in the DNA-binding domain. As a result, we refer to these two conformations as 'narrow' (exhibited by SmcR dimer AB) and 'wide' (exhibited by SmcR dimer CD). The two conformations are reminiscent of previously studied TetR-type proteins with a pendulum-like movement of the DNA-binding domain (41). The individual Cα distances between the wide and narrow dimers in the DNA binding domain range from ∼2 to 6 Å, whereas the average overall distances between individual Cα for comparing the wild-type wide and narrow dimers is 0.6 Å (Figure 4C). It is important to note that in all crystallographic studies a caveat is that conformational changes may be artifacts due to crystal packing. In addition, although we observe two conformations, we cannot rule out the possibility that the DNA binding domain dwells in additional conformations than the two captured in the crystal structures. Additional conformations could be intermediate states between the two conformations shown here or could be conformations sampling wider or narrower states than our solved structures.

The X-ray crystal structure of the SmcR N55I variant has a single conformation

We also used X-ray crystallography to examine the structure of SmcR N55I and determined the structure at 3.4 Å. Unfortunately, our attempts to improve the resolution, including the crystallization of His-tagged variants, were unsuccessful. We next superimposed the structure of SmcR N55I (6WAF) to wild-type SmcR 3KZ9 since both structures were generated from untagged proteins (39). These superimpositions were performed using the matchmaker function in Chimera, which considers the best alignment for the overall structure (Figure 5A). The algorithm can also consider the dimerization domains (the part of the protein suspected to have the least flexibility and lowest B-factor values) as the fixed region. However, we opted to utilize the matchmaker function in Chimera to analyze the data using the best overall fit to ensure less user bias. SmcR N55I has only one dimer in the asymmetric unit (6WAF; space

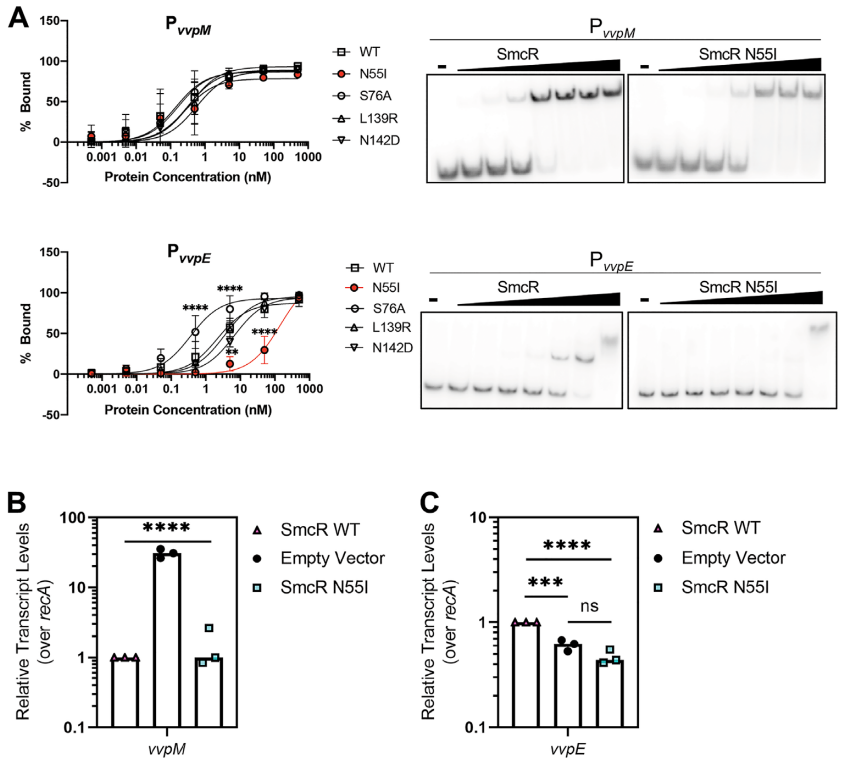

Figure 3. SmcR mutant N55I has limited DNA binding activity and transcriptional activation activity at P_{vvpE}. (**A**) EMSA reactions consisting of 0.5 nM radiolabeled DNA substrates (P_{vvpM}or P_{vvpE} binding sites on the top and bottom, respectively, with oligonucleotides listed in Table 1 and Supplementary Table S3) and increasing concentrations of purified wild-type SmcR or SmcR substitution mutant proteins (0.0005, 0.005, 0.05, 0.5, 5, 50, 500 nM protein). Data points show the average of three independent experiments, and error bars indicate the standard deviation. Representative gels of EMSA reactions are shown to the right. Lanes labeled '—' had no protein added. Asterisks indicate that the values (for N55I and S76A) are significantly different than the wild-type counterpart (**** $P < 0.0001$; ** $P = 0.01$; two-way analysis of variance (ANOVA), followed by Dunnett's multiple-comparison test; $n = 3$). (**B**, **C**) Relative transcript levels of *V. vulnificus* (B) *vvpM* and (C) *vvpE* determined by qRT-PCR of transcripts from *V. vulnificus* Δ*smcR* strains containing either a plasmid expressing *smcR* from an IPTG-inducible promoter (pJN22), *smcR* N55I (pJN27), or empty vector (pMMB67EH-kanR), induced with 50 μM IPTG. Asterisks indicate that the values are significantly different than the wild-type counterpart (ns = no significant difference; **** $P < 0.0001$; *** $P = 0.0005$; one-way ANOVA, followed by Tukey's multiple-comparison test; $n = 3$).

group C2). This dimer aligns best to the wide dimer of wild-type SmcR 3KZ9 and seems to be distinct from the SmcR 3KZ9 narrow dimer (Figure 5A). We quantified the structural differences by comparing the distances between alpha carbons in the SmcR N55I wide dimer to the SmcR 3KZ9 narrow dimer (Figure 5B, C) or SmcR 3KZ9 wide dimer (Figure 5D, E). The alignment of SmcR N55I to the SmcR 3KZ9 wide dimer plot shows little variation, with distances between alpha carbons generally less than 2 Å (Figure 5D, E). However, the SmcR N55I monomer A shows large (2–4 Å) variations in Cα compared to SmcR 3KZ9 monomer A in the narrow dimer in the DNA-binding domain residues 5–75 (Figure 5B), reminiscent of the variations observed between the wide and narrow dimers in SmcR wild-type (Figure 4C). The fluctuations in the other regions of the proteins are small (protein's overall Cα average = 0.76 Å), especially in flexible loop regions as expected (Figure 5B–E). It is noteworthy to mention that despite the low resolution at which SmcR N55I was solved, alpha-carbon distances estimated in this work are rather accurate. Hardly surprising, the side chains in low resolution structures are often mistakenly assigned due to the deficient electron-density maps in those regions. However, generally the electron-density for the protein backbone, as well as the alpha-carbon atoms assigned are more certain. Because the SmcR N55I structure was solved at a lower resolution, the *B*-factors are higher values compared to the SmcR wild-type structure (Supplementary Table S4). However, when considering the overall range of *B*-factors in the SmcR N55I structure, the relative values for the DNA binding domain compared to the dimerization domain are similar to that of wild-type (39). Together, these results indicate that the single SmcR N55I structure aligns closely with the wide conformation of wild-type SmcR. Importantly, we cannot rule out the influence of crystal contacts on conformational changes. We note that I55 in the SmcR N55I structure has contacts ∼4.1–4.4 Å with residues in the symmetry mate, which could affect the conformation.

SmcR forms multiple conformations in solution

To assess the conformations of SmcR in solution, we performed small-angle X-ray scattering (SAXS) experiments. Because SAXS data is obtained in solution without crystal lattice restraints, the structural information observed is likely more representative of the cellular environment. This is particularly important if a protein exists in multi-conformational or multimeric states. SAXS is useful in the

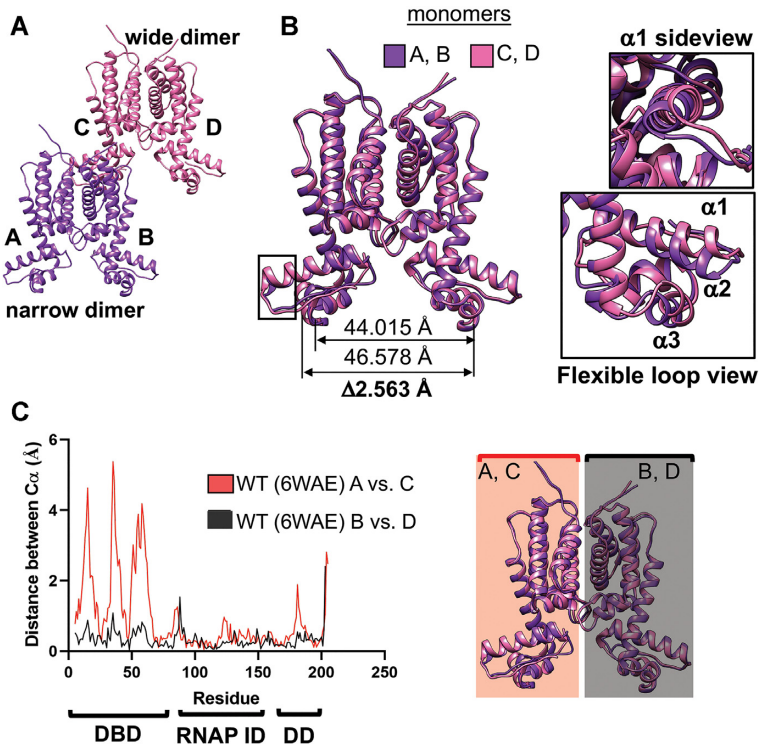

Figure 4. Wild-type SmcR has two DNA binding domain conformations. (**A**) The asymmetric unit containing two of the wild-type His-tagged SmcR dimers (6WAE; purple and pink). (**B**) Crystal structure of the his-tagged SmcR wild-type (PDB: 6WAE) monomers A and B that form the narrow dimer (purple) are superimposed to monomers C and D that form the wide dimer (pink). The distance between alpha carbons (Cα) at residue 55 between monomers A to B (narrow dimer) or between monomers C to D (wide dimer) is shown beneath the structure (A–B measurement above C-D measurement). Helices 1, 2 and 3 are shown in insets to the right. (**C**) Graph showing the Cα of his-tagged SmcR wild-type (PDB: 6WAE) between monomer A to monomer C (red) and between monomer B to monomer D (black), with a diagram shaded in red or black to show which dimers are compared in the Cα graph. DBD, DNA binding domain; RNAP ID, RNAP interaction domain; DD, dimerization domain.

composition analysis of mixtures using existing software and well-established protocols, provided that structural coordinates of low-symmetry conformers are known (62,65–67).

The SAXS data collected for wild-type SmcR were fit to the 6WAE X-ray crystal structures. The results of data fitting indicated the presence of both dimers and tetramers of SmcR in the absence of DNA (Table 2). This was unexpected because TetR tetramer formation that has been observed is DNA-dependent, with dimers binding opposing faces of DNA (43–46), while here we observe tetramers in the absence of DNA. The data fitting for the narrow dimer or wide dimer alone is very poor ($\chi^2 > 10$; Table 3; Supplementary Figure S7), suggesting that SmcR does not form dimers in a single conformation, but rather in combinations of conformations. The SmcR SAXS data have the best fit (lowest χ^2) to the combination of a wide dimer and a mixed tetramer with wide-narrow conformations, as compared to tetramers with wide-wide or narrow-narrow combinations (Figure 6A, Table 2).

The SmcR N55I SAXS analyses indicate the presence of higher-order structures, perhaps rods, in most samples with concentrations >1 mg/ml. At 1 mg/ml, the SmcR N55I SAXS data showed better fits to the wild-type 6WAE crystal structures compared to the 6WAF N55I structure with a combination of dimers and tetramers, similar to wild-type SmcR (Table 3; Supplementary Figure S8). This is likely because the N55I 6WAF structure has only the dimer in the asymmetric unit, and models of N55I tetramers with symmetry mates may not represent the tetramers observed in solution by SAXS. Thus, the N55I data fit better to the tetramers in 6WAE. As with wild-type, the fitting for N55I data to the narrow dimer or wide dimer alone is poor ($\chi^2 >$ 1.0; Table 3). Mixtures of narrow dimer or wide dimer combined with tetramers (of all combinations) produce similar χ^2 values (0.28–0.29), indicating that the data fit best to a mixture of dimers and tetramers. However, among the lowest χ^2 (best) fits, the highest volume fraction of the dimer is found in the wide conformation mixed with a tetramer in the wide-wide conformation (Figure 6B, Table 3). From these data, we conclude that wild-type SmcR exists in at least the two wide and narrow conformations in solution in a combination of dimers and tetramers. SmcR N55I may also exist in multiple conformations, but SAXS analyses suggest the best fit of these data is to wide dimer and wide-wide tetramer conformations, likely indicating that SmcR N55I exists in the wide conformation more frequently.

SmcR RNAP-interaction mutants have two-conformation structures similar to wild-type

The amino acid substitutions S76A, L139R and N142D in SmcR alpha helices 4 and 7 are predicted to be involved in protein-protein interactions based on previous research on

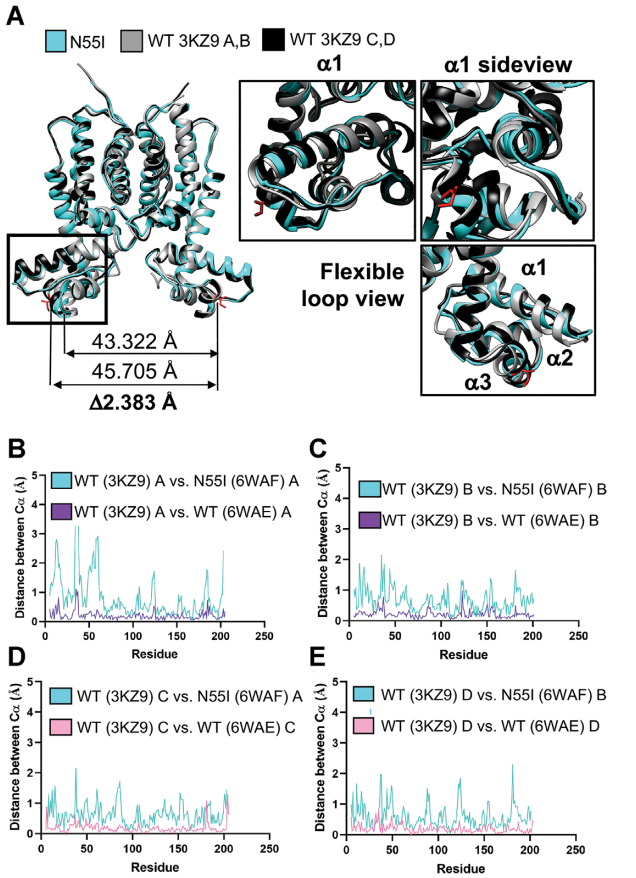

Figure 5. Crystal structure of SmcR N55I exists in the wide conformation. (**A**) The two dimers of SmcR 3KZ9 (narrow AB dimer, gray; wide CD dimer, black) and SmcR N55I dimer (cyan; 6WAF) superimposed. The insets show the superimposed α1, α2, and α3 helices and the connecting loop in the DNA binding domain. The distance between alpha carbons (Cα) at residue 55 between SmcR 3KZ9 monomers A to B (narrow dimer) or between SmcR N55I A to B (similar to WT C and D; wide dimer) is shown beneath the structure (3KZ9 measurement above N55I measurement). (B–E) Graphs of the Cα distances calculated by Chimera. Compared distances are as follows: (**B**) SmcR wild-type monomer A versus SmcR N55I monomer A (cyan), and SmcR 3KZ9 monomer A versus SmcR 6WAE monomer A (purple), (**C**) SmcR 3KZ9 wild-type monomer B versus SmcR N55I monomer B (cyan), and SmcR 3KZ9 monomer B versus SmcR 6WAE monomer B (purple), (**D**) SmcR wild-type monomer C versus SmcR N55I monomer A (cyan), and SmcR 3KZ9 monomer C versus SmcR 6WAE monomer C (pink), and (**E**) SmcR wild-type monomer D versus SmcR N55I monomer B (cyan), and SmcR 3KZ9 monomer D versus SmcR 6WAE monomer D (pink).

LuxR and HapR, given that these substitutions render the proteins unable to interact with RNAP alpha *in vitro* and are decreased in transcription activation (24). To determine whether these substitutions affect the structure of the protein, we solved the X-ray crystal structures of SmcR S76A, L139R, and N142D (resolutions of 2.57, 2.55 and 2.58 Å, respectively; PDB 6WAG, 6WAH, 6WAI). Each of the substitution mutants has two dimers in the asymmetric unit. These structures are highly similar to wild-type SmcR and show no appreciable change in alpha helices from the wild-type SmcR structure aside from movement in unstructured loops. The average overall alpha carbon distance between wild-type and the substitution mutants S76A, L139R, and N142D are 0.18, 0.25 and 0.17 Å, respectively (Supplementary Figure S5). Importantly, much like wild-type SmcR, each of the substitution mutants also show two DNA binding domain conformations (Figure 7A, C, E). The alpha carbon distances between the wide and narrow dimers for each substitution mutant show that the DNA binding domain alpha helices are also shifted, similar to wild-type SmcR (Figure 7B, D, F). From these structural data, we conclude that the S76A, L139R and N142D substitution mutants of SmcR have similar structures to wild-type SmcR and exist in multiple conformations.

Based on these data, we predicted that the DNA binding activity of these mutants is similar to wild-type SmcR. To test this, we used EMSAs to assay DNA binding at the *vvpE* and *vvpM* promoters for each substitution mutant compared to wild-type SmcR (Figure 3A, Supplementary Figure S6). The K_D of the RNAP-interaction substitution mutants with P_{vvpM} are not significantly different than wild-type or N55I. In addition, the affinities of the RNAP-interaction mutants L139R and N142D for P_{vvpE} are not significantly different than wild-type. However, S76A has a significantly increased binding affinity for P_{vvpE} (WT = 2.1 nM, S76A = 0.4 nM; $P < 0.01$). In contrast, the N55I K_D of 141.5 nM is a significantly much worse affinity compared to wild-type (32,68,69). From these data, we conclude that the substitutions in the RNAP-interaction domain do not alter the conformational structure of SmcR and do not decrease DNA binding activity. Thus, the decreased transcription activation observed *in vivo* is likely due to disrupted protein-protein interactions.

The SmcR N55 residue is predicted to interact with the major groove of the DNA

The DNA-bound structure of another TetR protein, QacR from *Staphylococcus aureus,* gives insight into putative structural shifts occurring in these proteins upon DNA binding (45,46). Due to interest in drug development, QacR has been highly studied with crystallography, making this a good candidate to compare a TetR protein crystallized in different conformations. Comparing the QacR-DNA structure to QacR-drug bound structures, we observed shifts in the DNA-binding domain (Figure 8A), similar to other TetR proteins that also have flexible DNA binding domains. Although the SmcR and QacR X-ray crystal structures indicate multiple conformations of these proteins, the wild-type HapR crystal structure (PDB: 2PBX) and an inactive DNA-binding HapR naturally occurring variant (G39D, $HapR_{V2}$; PDB: 6D7R) both only show one conformation in their crystal structures, which align closest to the wide SmcR conformation (40,70). However, another study using small/wide angle X-ray scattering (SWAXS) showed the G39D variant also has a change in DNA binding domain conformation (71). Because this technique is performed using protein in solution rather than crystallized protein, we have increased confidence that these conformational changes are not due to crystal packing artifacts.

Using the QacR-DNA structure as a guide, we investigated the predicted interactions of the SmcR DNA binding domain to DNA (Figure 8B). The QacR protein sequence

Table 2. SAXS analyses of wild-type SmcR

Data fit to SmcR 6WAE[a]							
Monomer narrow	Monomer wide	Dimer narrow	Dimer wide	Tetramer narrow-wide	Tetramer narrow-narrow	Tetramer wide-wide	χ^2
N/A	N/A	1	N/A	N/A	N/A	N/A	16.53
N/A	N/A	N/A	1	N/A	N/A	N/A	13.97
N/A	N/A	N/A	N/A	1	N/A	N/A	35.05
0	N/A	1	N/A	N/A	N/A	N/A	16.53
N/A	0	N/A	1	N/A	N/A	N/A	13.97
N/A	N/A	0.627±0.006	N/A	0.372±0.006	N/A	N/A	0.73
N/A	**N/A**	**N/A**	**0.646±0.006**	**0.354±0.006**	**N/A**	**N/A**	**0.68**[b]
N/A	N/A	0.000±0.000	0.646±0.006	0.354±0.006	N/A	N/A	0.68
N/A	N/A	0.636±0.006	N/A	N/A	N/A	0.364±0.006	0.77
N/A	N/A	N/A	0.654±0.007	N/A	N/A	0.345±0.006	0.72
N/A	N/A	0.000±0.000	0.654±0.007	N/A	N/A	0.345±0.006	0.72
N/A	N/A	0.628±0.006	N/A	N/A	0.372±0.006	N/A	0.80
N/A	N/A	N/A	0.646±0.006	N/A	0.354±0.006	N/A	0.74
N/A	N/A	0.000±0.000	0.646±0.006	N/A	0.354±0.006	N/A	0.74

[a]χ^2 values are listed in first column from right. The volume fractions of involved conformations are listed in rest columns.
[b]The data with the lowest χ^2 and best volume fits are shown in bold.

Table 3. SAXS analyses of SmcR N55I

Data fit to SmcR N55I 6WAF[a]							
Monomer	Dimer	Tetramer					χ^2
NA	1	NA					1.62
0	1	NA					1.62
NA	NA	1					1.69
Data fit to SmcR 6WAE[a]							
Monomer narrow	**Monomer wide**	**Dimer narrow**	**Dimer wide**	**Tetramer narrow-wide**	**Tetramer narrow-narrow**	**Tetramer wide-wide**	**χ^2**
NA	NA	1	NA	NA	NA	NA	1.53
NA	NA	NA	1	NA	NA	NA	1.32
NA	NA	NA	NA	1	NA	NA	3.72
0	NA	1	NA	NA	NA	NA	1.53
NA	0	NA	1	NA	NA	NA	1.32
NA	NA	0.672 ± 0.021	NA	0.328 ± 0.017	NA	NA	0.28
NA	NA	NA	0.690 ± 0.022	0.310 ± 0.018	NA	NA	0.28
NA	NA	0.672 ± 0.021	NA	NA	0.328 ± 0.017		0.29
NA	NA	0.680 ± 0.021	NA	NA		0.320 ± 0.017	0.29
NA	NA	NA	0.697 ± 0.022	NA	NA	0.303 ± 0.017	0.28
NA	NA	NA	0.690 ± 0.022	NA	0.310 ± 0.018	NA	0.28
NA	NA	0	0.690 ± 0.022	0.310 ± 0.018	NA	NA	0.28
NA	NA	0	0.690 ± 0.022	NA	0.310 ± 0.018	NA	0.28
NA	**NA**	**0**	**0.697 ± 0.022**	**NA**	**NA**	**0.303 ± 0.017**	**0.28**[b]

[a]χ^2 values are listed in first column from right. The volume fractions of involved conformations are listed in rest columns.
[b]The data with the lowest χ^2 and best volume fits are shown in bold.

is much different than SmcR (27% shared identity) but the quaternary structures are similar (RMSD of 3.1 Å) (72). Additionally, the DNA binding sequence of QacR is different than that of SmcR (Figure 8B), thus it is difficult to make direct comparisons of the QacR-DNA structure to SmcR to predict what amino acids contact nucleotides. However, alignment of the SmcR crystal structure to the QacR-DNA structure suggests that the residues V50, A51, F54 and N55 of SmcR may interact with bases in the major groove of the DNA (Figure 8C). Thus, substituting I55 for N55 could either clash with base-pairs or could prevent hydrogen bonding that N55 may normally participate in, however this cannot be determined in the absence of DNA-bound SmcR wild-type and N55I structures. Recently, one of the *Vibrio* TetR-type proteins has been successfully co-crystallized with DNA: *V. alginolyticus* LuxR (31). This was very helpful in further analyzing our hypothesis of N55 interactions because *V. alginolyticus* LuxR also has an N55 residue, and the binding site sequence is more similar to that of the SmcR binding site sequences used throughout this study (31). Comparing these interactions, we found that our predictions on contacts for *Vibrio* SmcR aligned well with contacts observed in the LuxR-DNA structures (Figure 8B). Interestingly, the LuxR N55 residues in both monomers contact the thymines on both sides of the palindromic repressed DNA sequence (3.4 and 3.5 Å). However, for the activated DNA sequence, the N55 residue on only one monomer contacts the thymine base at that position (3.3 Å), whereas N55 in the other monomer does not make the same contact with the adenine in the other half of the

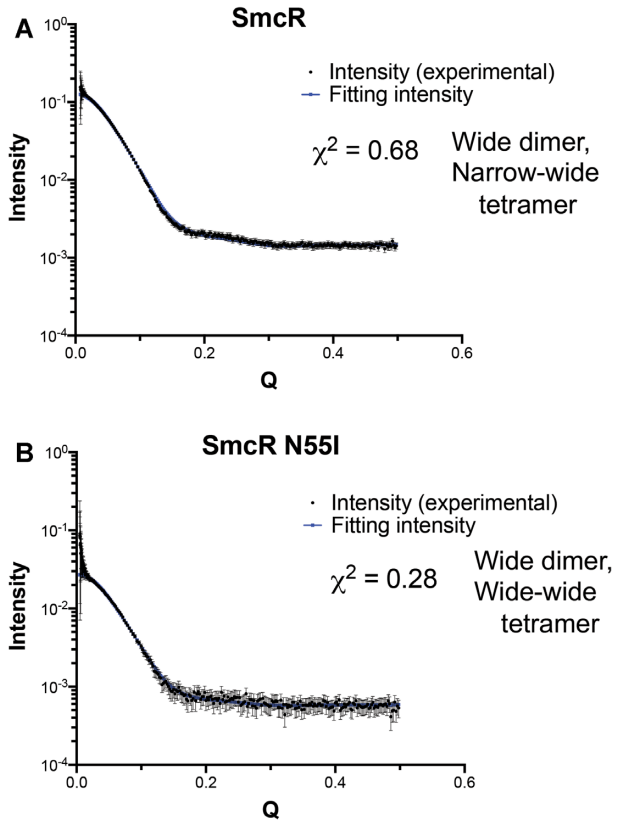

Figure 6. SAXS data fit to conformations of SmcR X-ray crystal structures. (**A**) Wild-type SmcR SAXS data were fit to varying combinations of SmcR 6WAE structures (Table 2). The best data fit to the combination of the wide dimer (CD dimer) and narrow-wide tetramer (AB, CD dimers) is shown. (**B**) SmcR N55I SAXS data were fit to varying combinations of SmcR structures using either 6WAE or 6WAF (Table 3). The best data fit to the combination of the wide dimer (CD dimer) and wide-wide tetramer (CD, CD dimers) from 6WAE is shown.

palindrome (31). This supports our findings that SmcR N55 is critical for recognition of different DNA sequences.

DISCUSSION

The study of transcriptional control of quorum-sensing genes is pivotal for a basic biological understanding of the evolution of coordinated behaviors, as well as for a better understanding of key drug targets to treat diseases coordinated by quorum sensing. Notably, LuxR/HapR/SmcR proteins are members of the TetR family of transcription factors that have diversified to bind more than 100 sites throughout the genome. This study has investigated how these regulators simultaneously maintain specificity for quorum-sensing targets and diversity to accommodate binding at numerous promoters for both activation and repression activities. The core importance of the work presented here is that the *Vibrio* family of LuxR/HapR/SmcR proteins have evolved from traditional TetR-type proteins and have the ability to activate transcription and to bind to numerous and diverse DNA sequences. Our model is that two biophysical properties enable these activities: (i) interaction with RNAP, which likely recruits or stabilizes RNAP at certain promoters and (ii) multiple DNA binding domain conformations that allow recognition of various sequences (Figure 9). While the hypothesis that LuxR/HapR/SmcR proteins adopt multiple conformations is not new, the biochemical, structural, and quantitative protein comparison data presented in this manuscript are the first to show definitive support for this model. The focus of this study has been solely on the biophysical mechanisms of activation and how specific SmcR-DNA and SmcR-protein interactions influence SmcR regulation of activated genes. We took advantage of known activation-deficient mutants to determine how these substitutions affected SmcR activity both *in vitro* and *in vivo*. Similar analyses could be performed to interrogate repression-deficient mutants to study whether similar SmcR-DNA interactions are vital for SmcR to function as a repressor (37).

Our structural studies from X-ray crystallography and SAXS have both shown that multiple structural conformations are adopted by SmcR to facilitate binding of variable DNA substrates in quorum-sensing promoters. Our findings align with well-documented observations of DNA binding domain 'plasticity' in several other TetR proteins from diverse bacteria in which the ligand binding domain has a pendulum-like motion (32,43). We hypothesize that the measurable alteration in the SmcR dimer between the two helix-turn-helix domains may enable SmcR to interact with DNA sequences from various promoters where sequence variation is restricted. For example, many LuxR binding sites have been shown to overlay the -35 region bound by sigma-70 (37,38,52). Limitations to changes in these regions may have driven selection for the protein to adapt to variable sequences, rather than mutations to the binding site itself.

We also observed that SmcR forms a mixture of dimers and tetramers in solution. This was unexpected because most TetR proteins are dimers in solution, or if a dimer of dimer formation is observed, then proteins bind DNA on opposing strands without neighboring proteins directly interacting. If SmcR adopts multiple conformations when bound to DNA versus unbound, this would fit other data in the field: the crystal structure of the TetR-type protein QacR bound to DNA exhibits a different conformation to that of QacR bound to ligands or inhibitors (44–46,73).

There are several plausible models for the mechanism that limits DNA binding by the N55I protein. The N55I substitution may have a limited range of sequence recognition due to a limited flexibility in its DNA binding domain. It is also possible that the substitution of isoleucine for asparagine restricts nucleotide recognition and any potential hydrogen binding that may be occurring, thus limiting base-specific contacts made by SmcR. We note that the sequences bound by SmcR N55I represent sites at which LuxR has been shown to have the tightest binding affinity (e.g. P_{luxC} site H and P_{05222}) (37). This could indicate that LuxR/HapR/SmcR proteins have evolved to be increasingly flexible to accommodate more binding sites for an expanded regulon compared to traditional TetR-type proteins. Another model is that SmcR forms either dimers or tetramers depending on the type of promoter, and N55I may be altered in its binding mode. These models could be addressed with in-solution structural experiments such as NMR to further understand the structural differences

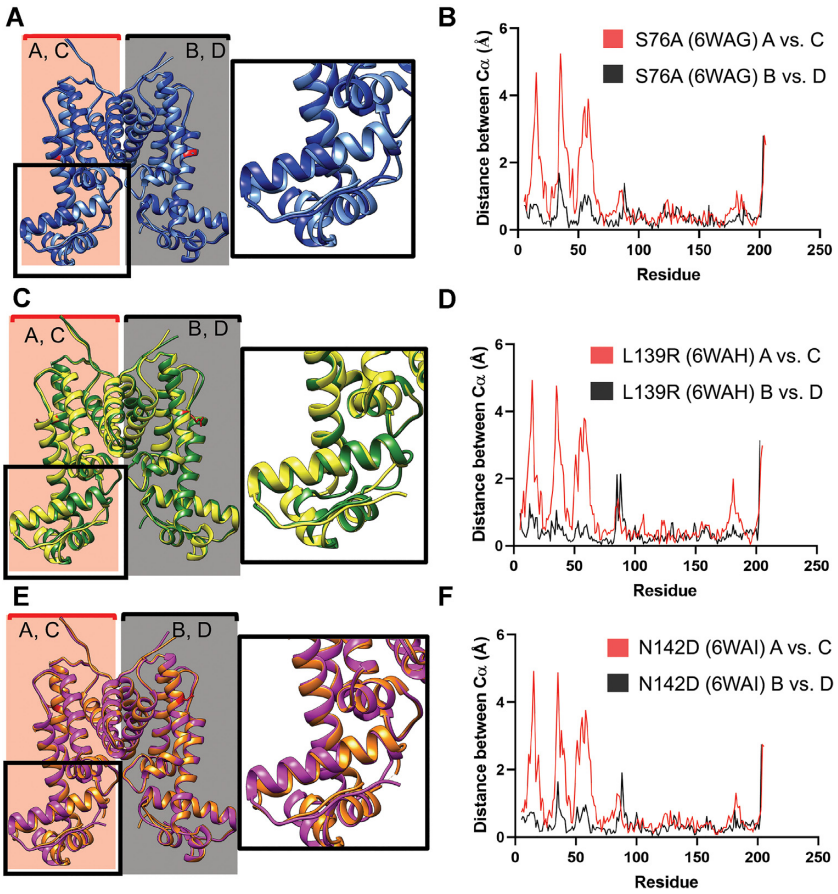

Figure 7. SmcR S76A, L139R and N142D exhibit structures similar to wild-type with two DNA binding domain conformations. (**A**) SmcR S76A (6WAG) narrow dimer (cornflower blue) structure aligned to the wide dimer (royal blue) with an inset zoomed into one monomer of the DNA binding domain. (**B**) Graph showing the Chimera measured distances between alpha carbons (Cα) of his-tagged SmcR S76A (PDB: 6WAG) from monomer A to monomer C (red) and from monomer B to monomer D (black). (**C**) SmcR L139R (6WAH) narrow dimer (forest green) structure aligned to the wide dimer (yellow) with an inset zoomed into one monomer of the DNA binding domain. (**D**) Graph showing the Cα of his-tagged SmcR L139R (PDB: 6WAH) from monomer A to monomer C (red) and from monomer B to monomer D (black). (**E**) SmcR N142D (6WAI) narrow dimer (orange) structure aligned to the wide dimer (magenta) with an inset zoomed into one monomer of the DNA binding domain. (**F**) Graph showing the Cα of his-tagged SmcR N142D (PDB: 6WAI) from monomer A to monomer C (red) and from monomer B to monomer D (black).

in these proteins. The DNA-bound SmcR and SmcR N55I structures would truly contribute the greatest information in DNA binding site recognition, though numerous attempts with various DNA substrates, SmcR protein purification schemes, and a library of crystallization conditions has not yet yielded crystals that diffract. Fortunately, the recent *V. alginolyticus* LuxR-DNA crystal structures have provided insight into mechanisms of DNA sequence recognition (31). The study by Zhang *et al.* shows the importance of N-terminal contacts with the minor groove that differ between activated and repressed sites, specifically residues R9 and R11 (31). In addition, the N55 residue makes specific nucleobase contacts in both monomers with the thymines in the repressed site, but only one monomer makes this contact in the activated site. Thus, the results presented by Zhang *et al.* (31) and this manuscript show that DNA binding site recognition in the LuxR/SmcR family of proteins relies on at least two mechanisms: (i) a flexible HTH that differs in nucleobase interactions and (ii) N-terminal minor groove interactions.

Ultimately, information regarding the mechanism of transcriptional regulation of the LuxR/HapR/SmcR family of proteins will inform future studies aiming to disrupt these pathways to mitigate pathogenesis regulated by quorum sensing (74,75). Specifically, the protein-protein and protein-DNA interactions required for function in these regulators represents a key target for small molecule inhibitors. Numerous small molecule inhibitor studies have been carried out targeting QacR (73). Notably, structures of QacR bound to molecules that inhibit QacR function have a wider conformation than the DNA-bound QacR, which supports our model that wide conformations have a more limited function *in vivo* (Figure 8). Similarly, studies in vibrios have produced some small molecule inhibitors with promising inhibitory effects on LuxR/HapR/SmcR, such as Qstatin, which limits transcription regulation by SmcR *in vivo* (17,76,77). The Qstatin-bound SmcR structure also exhibits the same two conformations in the DNA binding domain, suggesting that the mechanism of Qstatin inhibition is not due to limitation of DNA binding sequence recogni-

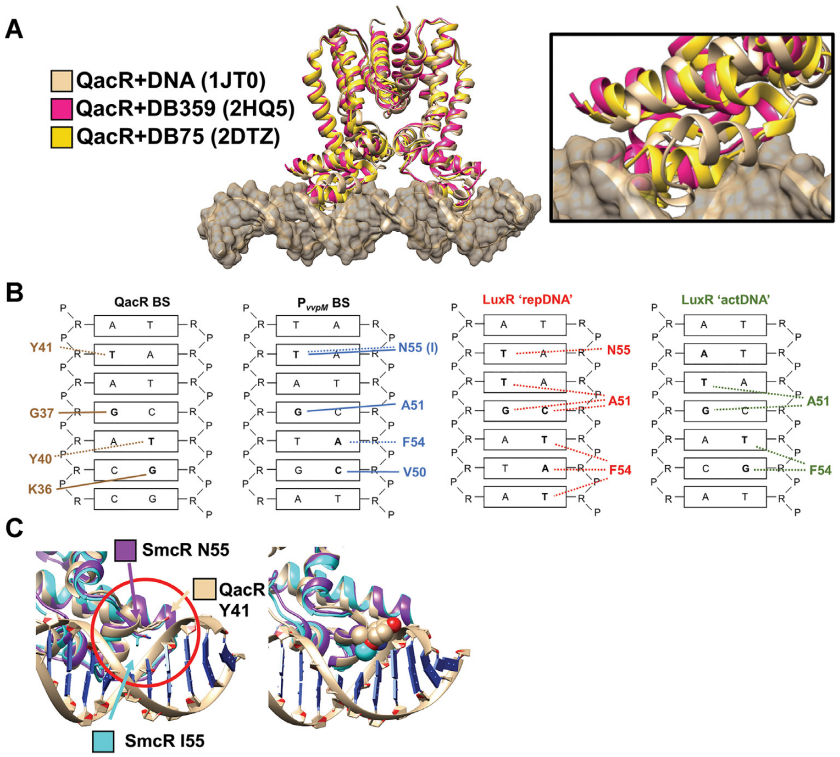

Figure 8. Structural comparisons of homologous TetR family proteins. (**A**) The structure of QacR and DNA (tan; 1JT0) is superimposed with QacR bound to inhibitors DB359 (pink; 2HQ5) and DB75 (gold; 2DTZ). The inset shows a zoomed-in view of the DNA-binding domain. (**B**) The DNA binding sites (BS) are shown for *S. aureus* QacR at the QacR site (45), *V. vulnificus* SmcR at the P_{vvpM}site, *V. alginolyticus* LuxR at a repressed site (repDNA), and *V. alginolyticus* LuxR at an activated site (actDNA) (31). Residues that interact with the bases via hydrogen (solid line) or van Der Waals (dotted line) interactions are shown. For QacR, LuxR-repDNA, and LuxR-actDNA, the interactions shown are derived from structures 1JT0, 7AMN and 7AMT, respectively. For SmcR, the putative interactions between SmcR residues and the bases in P_{vvpM} (blue) are drawn based on the alignment of wild-type SmcR (6WAE) to the QacR-DNA structure (1JT0). (**C**) The aligned QacR-DNA (tan; 1JT0)), SmcR WT (purple; 6WAE) and SmcR N55I (cyan; 6WAF) are shown with the aligned residue of interest (QacR Y = tyrosine SmcR WT N = asparagine, and SmcR N55I = isoleucine) in the DNA-binding domain shown in stick representation (left) or space filling representation (right).

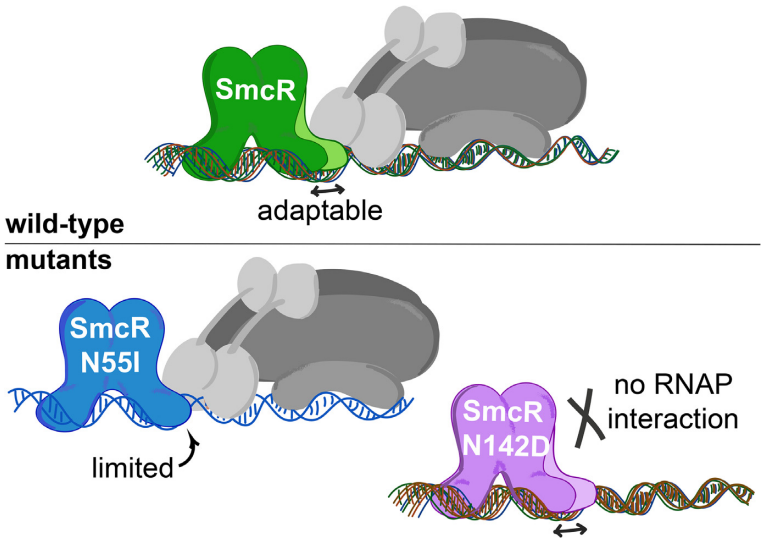

Figure 9. Model: Multiple SmcR DNA binding domain conformations accommodate a wide array of DNA substrates. The DNA binding domain in SmcR is flexible and exhibits at least two conformations in crystal structures, enabling recognition of numerous DNA sequences. Mutant proteins have loss-of-function transcriptional phenotypes due to either (i) limited sequence recognition (e.g. N55I) or (ii) disrupted interaction with RNAP but maintained DNA binding activity (e.g. N142D).

tion. Further mechanistic studies will be required to determine the way by which Qstatin inhibits SmcR function *in vivo*.

DATA AVAILABILITY

X-ray crystallography structure data are available in the RCSB Protein Data Bank files 6WAE, 6WAF, 6WAG, 6WAH and 6WAI. SAXS data and models are available in the Small Angle Scattering Biological Data Bank files SASDKD8 and SASDKE8.

SUPPLEMENTARY DATA

Supplementary Data are available at NAR Online.

ACKNOWLEDGEMENTS

The authors gratefully acknowledge use of the Macromolecular Crystallography Facility (MCF) in the Molecular and Cellular Biochemistry Department, Indiana University Bloomington. We thank Dr. Susanne Ressl for advice on data analysis and suggestions on the manuscript. We also thank Jay Nix for his assistance during X-ray data collection at beamline 4.2.2, ALS. We acknowledge the use of the SAXS Core Facility of the Center for Cancer Research in the National Cancer Institute (NCI) of the National Institutes of Health (NIH). The content of this publication does not necessarily reflect the views or policies of the Department of Health and Human Services, nor does mention of trade names, commercial products, or organizations imply endorsement by the U.S. Government. The SAXS data were collected at beamline 12-ID-B of Advanced Photon Source (APS) of Argonne National Laboratory (ANL). We thank Dr Xiaobing Zuo at ANL for assistance during SAXS data collection. The content is solely the responsibility of the authors and does not necessarily represent the official views of the NIH.
Author contributions: J.N., L.F. and J.V.K. designed the experiments, J.N., M.R., L.F., G.G.G. and J.V.K. performed experiments, J.N., L.F., Y.X.W., G.G.G. and J.V.K. analyzed results and J.N., G.G.G., Y.X.W. and J.V.K. wrote the manuscript.

FUNDING

NIH [R35GM124698 to J.V.K.]; Indiana Clinical and Translational Science Institute (CTSI) [UL1TR002529, in part] from the NIH, National Center for Advancing Translational Sciences, Clinical and Translational Sciences Award; NCI SAXS core resource has been funded in whole or in part with federal funds from NCI [HHSN26120080001E]; Intramural Research Program of the NIH, National Cancer Institute, Center for Cancer Research; use of the APS was supported by the U.S. Department of Energy, Office of Science, Office of Basic Energy Sciences [DE-AC02-06CH11357]. Funding for open access charge: NIH/NIGMS [R35GM124698].
Conflict of interest statement. None declared.

REFERENCES

1. Miller,M.B., Skorupski,K., Lenz,D.H., Taylor,R.K. and Bassler,B.L. (2002) Parallel quorum sensing systems converge to regulate virulence in vibrio cholerae. *Cell*, **110**, 303–314.
2. Ellison,C.K., Dalia,T.N., Vidal Ceballos,A., Wang,J.C.-Y., Biais,N., Brun,Y. V. and Dalia,A.B. (2018) Retraction of DNA-bound type IV competence pili initiates DNA uptake during natural transformation in Vibrio cholerae. *Nat. Microbiol.*, **3**, 773–780.
3. Pena,R.T., Blasco,L., Ambroa,A., González-Pedrajo,B., Fernández-García,L., López,M., Bleriot,I., Bou,G., García-Contreras,R., Wood,T.K. *et al.* (2019) Relationship between quorum sensing and secretion systems. *Front. Microbiol.*, **10**, 1100.
4. Henke,J. and Bassler,B. (2004) Quorum sensing regulates type III secretion in *Vibrio harveyi* and *Vibrio parahaemolyticus*. *J. Bacteriol.*, **186**, 3794–3805.
5. McRose,D.L., Baars,O., Seyedsayamdost,M.R., Morel,F.M.M., Butler,A. and Harwood,C.S. (2018) Quorum sensing and iron regulate a two-for-one siderophore gene cluster in Vibrio harveyi. *Proc. Natl Acad. Sci. U.S.A.*, **115**, 7581–7586.
6. Guillemette,R., Ushijima,B., Jalan,M., Häse,C.C. and Azam,F. (2020) Insight into the resilience and susceptibility of marine bacteria to T6SS attack by Vibrio cholerae and Vibrio coralliilyticus. *PLoS One*, **15**, e0227864.
7. Paranjpye,R.N. and Strom,M.S. (2005) Colonization of shellfish by pathogenic Vibrios. *Proc. MTS/IEEE Oceans*, **2**, 1099–1103.
8. Soto-Rodriguez,S.A., Gomez-Gil,B., Lozano-Olvera,R., Betancourt-Lozano,M. and Morales-Covarrubias,M.S. (2015) Field and experimental evidence of Vibrio parahaemolyticus as the causative agent of acute hepatopancreatic necrosis disease of cultured shrimp (*Litopenaeus vannamei*) in northwestern Mexico. *Appl. Environ. Microbiol.*, **81**, 1689–1699.
9. Jayasree,L., Janakiram,P. and Madhavi,R. (2006) Characterization of *Vibrio* spp. Associated with Diseased Shrimp from Culture Ponds of Andhra Pradesh (India). *J. World Aquac. Soc.*, **37**, 523–532.
10. Fadel,H.M. and El-Lamie,M.M.M. (2019) Vibriosis and Aeromonas infection in shrimp: isolation, sequencing, and control. *Int. J. One Heal.*, **5**, 38–48.
11. Fuqua,W.C., Winans,S.C. and Greenberg,E.P. (1994) Quorum sensing in bacteria: The LuxR-LuxI family of cell density- responsive transcriptional regulators. *J. Bacteriol.*, **176**, 269–275.
12. Fuqua,C., Winans,S.C. and Greenberg,E.P. (1996) Census and consensus in bacterial ecosystems: the LuxR-LuxI family of quorum-sensing transcriptional regulators. *Annu. Rev. Microbiol*, **50**, 727–751.
13. Waters,C.M. and Bassler,B.L. (2005) Quorum sensing: communication in bacteria. *Annu. Rev. Cell Dev. Biol.*, **21**, 319–346.
14. Teng,S.W., Wang,Y., Tu,K.C., Long,T., Mehta,P., Wingreen,N.S., Bassler,B.L. and Ong,N.P. (2010) Measurement of the copy number of the master quorum-sensing regulator of a bacterial cell. *Biophys. J.*, **98**, 2024–2031.
15. Liu,Z., Hsiao,A., Joelsson,A. and Zhu,J. (2006) The transcriptional regulator VqmA increases expression of the quorum-sensing activator HapR in *Vibrio cholerae*. *J. Bacteriol.*, **188**, 2446–2453.
16. Kim,S.M., Park,J.H., Lee,H.S., Kim,W. Bin, Ryu,J.M., Han,H.J. and Choi,S.H. (2013) LuxR homologue SmcR is essential for *Vibrio vulnificus* pathogenesis and biofilm detachment, and its expression is induced by host cells. *Infect. Immun.*, **81**, 3721–3730.
17. Kim,B.S., Jang,S.Y., Bang,Y.-J., Hwang,J., Koo,Y., Jang,K.K., Lim,D., Kim,M.H. and Choi,S.H. (2018) QStatin, a selective inhibitor of quorum sensing in *Vibrio* species. *MBio*, **9**, e02262-17.
18. Lin,B., Wang,Z., Malanoski,A.P., O'Grady,E.A., Wimpee,C.F., Vuddhakul,V., Alves,N., Thompson,F.L., Gomez-Gil,B. and Vora,G.J. (2010) Comparative genomic analyses identify the *Vibrio harveyi* genome sequenced strains BAA-1116 and HY01 as Vibrio campbellii. *Environ. Microbiol. Rep.*, **2**, 81–89.
19. Freeman,J.A. and Bassler,B.L. (1999) Sequence and function of LuxU: a two-component phosphorelay protein that regulates quorum sensing in Vibrio harveyi. *J. Bacteriol.*, **181**, 899–906.
20. Anetzberger,C., Reiger,M., Fekete,A., Schell,U., Stambrau,N., Plener,L., Kopka,J., Schmitt-Kopplin,P., Hilbi,H. and Jung,K. (2012) Autoinducers act as biological timers in *Vibrio harveyi*. *PLoS One*, **7**, e48310.

21. Simpson,C.A., Podicheti,R., Rusch,D.B., Dalia,A.B. and van Kessel,J.C. (2019) Diversity in natural transformation frequencies and regulation across vibrio species. *MBio*, **10**, e02788-19.
22. Jones,M.K. and Oliver,J.D. (2009) Vibrio vulnificus: Disease and pathogenesis. *Infect. Immun.*, **77**, 1723–1733.
23. Kim,C.-M., Park,R.-Y., Chun,H.-J., Kim,S.-Y., Rhee,J.-H. and Shin,S.-H. (2007) *Vibrio vulnificus* metalloprotease VvpE is essentially required for swarming. *FEMS Microbiol. Lett.*, **269**, 170–179.
24. Ball,A.S. and van Kessel,J.C. (2019) The master quorum sensing regulators LuxR/HapR directly interact with the alpha subunit of RNA polymerase to drive transcription activation in *Vibrio harveyi* and *Vibrio cholerae*. *Mol. Microbiol.*, **111**, 1317–1334.
25. Jeong,H.S., Kim,S.M., Lim,M.S., Kim,K.S. and Choi,S.H. (2010) Direct interaction between quorum-sensing regulator SmcR and RNA polymerase is mediated by integration host factor to activate vvpE encoding elastase in Vibrio vulnificus. *J. Biol. Chem.*, **285**, 9357–9366.
26. Savery,N.J., Lloyd,G.S., Kainz,M., Gaal,T., Ross,W., Ebright,R.H., Gourse,R.L. and Busby,S.J.W. (1998) Transcription activation at Class II CRP-dependent promoters: identification of determinants in the C-terminal domain of the RNA polymerase α subunit. *EMBO J.*, **17**, 3439–3447.
27. Lee,D.J., Minchin,S.D. and Busby,S.J.W. (2012) Activating transcription in bacteria. *Annu. Rev. Microbiol*, **66**, 125–152.
28. Browning,D.F. and Busby,S.J.W. (2004) The regulation of bacterial transcription initiation. *Nat. Rev.*, **2**, 57–65.
29. Philips,S.J., Canalizo-Hernandez,M., Yildirim,I., Schatz,G.C., Mondragón,A. and O'Halloran,T.V. (2015) Allosteric transcriptional regulation via changes in the overall topology of the core promoter. *Science (80-.).*, **349**, 877–881.
30. Jutras,B.L., Verma,A. and Stevenson,B. (2012) Identification of novel DNA-binding proteins using DNA-affinity chromatography/pull down. *Curr. Protoc. Microbiol.*, doi:10.1002/9780471729259.mc01f01s24.
31. Zhang,J., Liu,B., Gu,D., Hao,Y., Chen,M., Ma,Y., Zhou,X., Reverter,D., Zhang,Y. and Wang,Q. (2021) Binding site profiles and N-terminal minor groove interactions of the master quorum-sensing regulator LuxR enable flexible control of gene activation and repression. *Nucleic Acids Res.*, **49**, 3274–3293.
32. Ramos,J.L., Martínez-Bueno,M., Molina-Henares,A.J., Terán,W., Watanabe,K., Zhang,X., Gallegos,M.T., Brennan,R. and Tobes,R. (2005) The TetR family of transcriptional repressors. *Microbiol. Mol. Biol. Rev.*, **69**, 326–356.
33. Li,W. and He,Z.G. (2012) LtmA, a novel cyclic di-GMP-responsive activator, broadly regulates the expression of lipid transport and metabolism genes in Mycobacterium smegmatis. *Nucleic Acids Res.*, **40**, 11292–11307.
34. Lee,D.H., Jeong,H.S., Jeong,H.G., Kim,K.M., Kim,H. and Choi,S.H. (2008) A consensus sequence for binding of SmcR, a *Vibrio vulnificus* LuxR homologue, and genome-wide identification of the SmcR regulon. *J. Biol. Chem.*, **283**, 23610–23618.
35. Lin,W., Kovacikova,G. and Skorupski,K. (2005) Requirements for *Vibrio cholerae* HapR binding and transcriptional repression at the hapR promoter are distinct from those at the aphA promoter. *J. Bacteriol.*, **187**, 3013–3019.
36. Tsou,A.M., Cai,T., Liu,Z., Zhu,J. and Kulkarni,R.V. (2009) Regulatory targets of quorum sensing in *Vibrio cholerae*: evidence for two distinct HapR-binding motifs. *Nucleic Acids Res.*, **37**, 2747–2756.
37. van Kessel,J.C., Ulrich,L.E., Zhulin,I.B. and Bassler,B.L. (2013) Analysis of activator and repressor functions reveals the requirements for transcriptional control by LuxR, the master regulator of quorum sensing in Vibrio harveyi. *MBio*, **4**, e00378-13.
38. Pompeani,A.J., Irgon,J.J., Berger,M.F., Bulyk,M.L., Wingreen,N.S. and Bassler,B.L. (2008) The *Vibrio harveyi* master quorum-sensing regulator, LuxR, a TetR-type protein is both an activator and a repressor: DNA recognition and binding specificity at target promoters. *Mol. Microbiol.*, **70**, 76–88.
39. Kim,Y., Kim,B.S., Park,Y.J., Choi,W.C., Hwang,J., Kang,B.S., Oh,T.K., Choi,S.H. and Kim,M.H. (2010) Crystal structure of SmcR, a quorum-sensing master regulator of *Vibrio vulnificus*, provides insight into its regulation of transcription. *J. Biol. Chem.*, **285**, 14020–14030.
40. De Silva,R.S., Kovacikova,G., Lin,W., Taylor,R.K., Skorupski,K. and Kull,F.J. (2007) Crystal structure of the *Vibrio cholerae* quorum-sensing regulatory protein HapR. *J. Bacteriol.*, **189**, 5683–5691.
41. Bhukya,H. and Anand,R. (2017) TetR regulators: a structural and functional perspective. *J. Indian Inst. Sci.*, **97**, 245–259.
42. Bhukya,H., Bhujbalrao,R., Bitra,A. and Anand,R. (2014) Structural and functional basis of transcriptional regulation by TetR family protein CprB from S. coelicolor A3(2). *Nucleic Acids Res.*, **42**, 10122–10133.
43. Tonthat,N.K., Milam,S.L., Chinnam,N., Whitfill,T., Margolin,W. and Schumacher,M.A. (2013) SlmA forms a higher-order structure on DNA that inhibits cytokinetic Z-ring formation over the nucleoid. *Proc. Natl. Acad. Sci. U.S.A.*, **110**, 10586–10591.
44. Grkovic,S., Brown,M.H., Schumacher,M.A., Brennan,R.G. and Skurray,R.A. (2001) The *Staphylococcal* QacR multidrug regulator binds a correctly spaced operator as a pair of dimers. *J. Bacteriol.*, **183**, 7102–7109.
45. Schumacher,M.A., Miller,M.C., Grkovic,S., Brown,M.H., Skurray,R.A. and Brennan,R.G. (2002) Structural basis for cooperative DNA binding by two dimers of the multidrug-binding protein QacR. *EMBO J.*, **21**, 1210–1218.
46. Schumacher,M.A. and Brennan,R.G. (2003) Deciphering the molecular basis of multidrug recognition: crystal structures of the Staphylococcus aureus multidrug binding transcription regulator QacR. *Res. Microbiol.*, **154**, 69–77.
47. Shiu-Hin Chan,D., Seetoh,W.G., McConnell,B.N., Matak-Vinković,D., Thomas,S.E., Mendes,V., Blaszczyk,M., Coyne,A.G., Blundell,T.L. and Abell,C. (2017) Structural insights into the EthR-DNA interaction using native mass spectrometry. *Chem. Commun.*, **53**, 3527–3530.
48. Shah,I.M. and Wolf,R.E. (2004) Novel protein-protein interaction between *Escherichia coli* SoxS and the DNA binding determinant of the RNA polymerase α subunit: SoxS functions as a co-sigma factor and redeploys RNA polymerase from UP-element-containing promoters to SoxS-dependent promot. *J. Mol. Biol.*, **343**, 513–532.
49. Gosink,K.K., Gaal,T., Bokal,A.J. IV and Gourse,R.L. (1996) A positive control mutant of the transcription activator protein FIS. *J. Bacteriol.*, **178**, 5182–5187.
50. Eschenlauer,A.C. and Reznikoff,W.S. (1991) Escherichia coli catabolite gene activator protein mutants defective in positive control of lac operon transcription. *J. Bacteriol.*, **173**, 5024–5029.
51. Rutherford,S.T., Van Kessel,J.C., Shao,Y. and Bassler,B.L. (2011) AphA and LuxR/HapR reciprocally control quorum sensing in vibrios. *Genes Dev.*, **25**, 397–408.
52. Chaparian,R.R., Olney,S.G., Hustmyer,C.M., Rowe-Magnus,D.A. and van Kessel,J.C. (2016) Integration host factor and LuxR synergistically bind DNA to coactivate quorum-sensing genes in Vibrio harveyi. *Mol. Microbiol.*, **101**, 823–840.
53. Newman,J.D. and van Kessel,J.C. (2020) Purification of the Vibrio quorum-sensing transcription factors LuxR, HapR, and SmcR. *Methods Mol. Biol.*, doi:10.1007/7651_2020_306.
54. Kabsch,W. (2010) XDS. *Acta Crystallogr. Sect. D Biol. Crystallogr.*, **66**, 125–132.
55. Emsley,P., Lohkamp,B., Scott,W.G. and Cowtan,K. (2010) Features and development of Coot. *Acta Crystallogr. Sect. D Biol. Crystallogr.*, **66**, 486–501.
56. Adams,P.D., Afonine,P. V., Bunkóczi,G., Chen,V.B., Davis,I.W., Echols,N., Headd,J.J., Hung,L.W., Kapral,G.J., Grosse-Kunstleve,R.W. *et al.* (2010) PHENIX: a comprehensive Python-based system for macromolecular structure solution. *Acta Crystallogr. Sect. D Biol. Crystallogr.*, **66**, 213–221.
57. Pettersen,E.F., Goddard,T.D., Huang,C.C., Couch,G.S., Greenblatt,D.M., Meng,E.C. and Ferrin,T.E. (2004) UCSF Chimera - a visualization system for exploratory research and analysis. *J. Comput. Chem.*, **25**, 1605–1612.
58. Schrödinger,L. (2015) In: The PyMOL Molecular Graphics System, Version 2.0.
59. Svergun,D.I. (1992) Determination of the regularization parameter in indirect-transform methods using perceptual criteria. *J. Appl. Crystallogr.*, **25**, 495–503.
60. Rambo,R.P. and Tainer,J.A. (2013) Accurate assessment of mass, models and resolution by small-angle scattering. *Nature*, **496**, 477–481.

61. Hajizadeh,N.R., Franke,D., Jeffries,C.M. and Svergun,D.I. (2018) Consensus Bayesian assessment of protein molecular mass from solution X-ray scattering data. *Sci. Rep.*, **8**, 7204.
62. Konarev,P.V, Volkov,V.V, Sokolova,A.V, Koch,M.H.J. and Svergun,D.I. (2003) PRIMUS: a Windows PC-based system for small-angle scattering data analysis. ¯ *PRIMUS J. Appl. Cryst*, **36**, 1277–1282.
63. Lee,M.-A., Kim,J.-A., Yang,Y.J., Shin,M.-Y., Park,S.-J. and Lee,K.-H. (2014) VvpM, an extracellular metalloprotease of Vibrio vulnificus, induces apoptotic death of human cells. *J. Microbiol.*, **52**, 1036–1043.
64. Shao,C.P. and Hor,L.I. (2001) Regulation of metalloprotease gene expression in Vibrio vulnificus by a Vibrio harveyi LuxR homologue. *J. Bacteriol.*, **183**, 1369–1375.
65. De Marco,V., Gillespie,P.J., Li,A., Karantzelis,N., Christodoulou,E., Klompmaker,R., Van Gerwen,S., Fish,A., Petoukhov,M.V., Iliou,M.S. *et al.* (2009). Quaternary structure of the human Cdt1-Geminin complex regulates DNA replication licensing. *Proc. Natl Acad. Sci. U.S.A.*, **106**, 19807–19812.
66. Korasick,D.A. and Tanner,J.J. (2018) Determination of protein oligomeric structure from small-angle X-ray scattering. *Protein Sci.*, **27**, 814–824.
67. Nagel,N., Graewert,M.A., Gao,M., Heyse,W., Jeffries,C.M., Svergun,D. and Berchtold,H. (2019) The quaternary structure of insulin glargine and glulisine under formulation conditions. *Biophys. Chem.*, **253**, 106226.
68. Azam,T.A. and Ishihama,A. (1999) Twelve species of the nucleoid-associated protein from *Escherichia coli*. Sequence recognition specificity and DNA binding affinity. *J. Biol. Chem.*, **274**, 33105–33113.
69. Chaparian,R.R., Tran,M.L.N., Miller Conrad,L.C., Rusch,D.B. and Van Kessel,J.C. (2020) Global H-NS counter-silencing by LuxR activates quorum sensing gene expression. *Nucleic Acids Res.*, **48**, 171–183.
70. Cruite,J., Succo,P., Raychaudhuri,S. and Kull,F.J. (2018) Crystal structure of an inactive variant of the quorum-sensing master regulator HapR from the protease-deficient non-O1, non-O139 *Vibrio cholerae* strain V2. *Acta Crystallogr. Sect. F, Struct. Biol. Commun.*, **74**, 331–336.
71. Dongre,M., Santa Singh,N., Dureja,C., Peddada,N., Solanki,A.K. and Raychaudhuri,S. (2011) Evidence on how a conserved glycine in the hinge region of HapR regulates its DNA binding ability lessons from a natural variant. *J. Biol. Chem.*, **286**, 15043.
72. Ball,A.S., Chaparian,R.R. and van Kessel,J.C. (2017) Quorum sensing gene regulation by LuxR/HapR master regulators in vibrios. *J. Bacteriol.*, **199**, e00105-17.
73. Brooks,B.E., Piro,K.M. and Brennan,R.G. (2007) Multidrug-binding transcription factor QacR binds the bivalent aromatic diamidines DB75 and DB359 in multiple positions. *J. Am. Chem. Soc.*, **129**, 8389–8395.
74. Brackman,G., Celen,S., Hillaert,U., van Calenbergh,S., Cos,P., Maes,L., Nelis,H.J. and Coenye,T. (2011) Structure-activity relationship of cinnamaldehyde analogs as inhibitors of AI-2 based quorum sensing and their effect on virulence of Vibrio spp. *PLoS One*, **6**. e16084.
75. Kratochvil,M.J., Yang,T., Blackwell,H.E. and Lynn,D.M. (2017) Nonwoven polymer nanofiber coatings that inhibit quorum sensing in *Staphylococcus aureus*: toward new nonbactericidal approaches to infection control. *ACS Infect. Dis.*, **3**, 271–280.
76. Brackman,G., Defoirdt,T., Miyamoto,C., Bossier,P., Van Calenbergh,S., Nelis,H. and Coenye,T. (2008) Cinnamaldehyde and cinnamaldehyde derivatives reduce virulence in Vibrio spp. by decreasing the DNA-binding activity of the quorum sensing response regulator LuxR. *BMC Microbiol.*, **8**, 149.
77. Defoirdt,T., Benneche,T., Brackman,G., Coenye,T., Sorgeloos,P. and Scheie,A.A. (2012) A quorum sensing-disrupting brominated thiophenone with a promising therapeutic potential to treat luminescent vibriosis. *PLoS One*, **7**, e41788.